HANSER

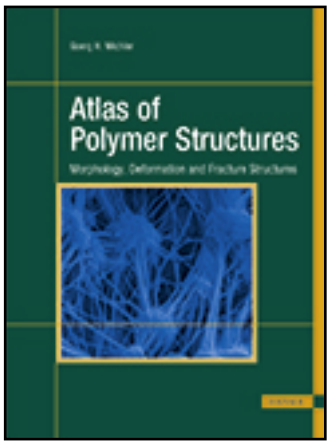

Sample Pages

Goerg H. Prof. Dr. Michler

Atlas of Polymer Structures

Morphology, Deformation and Fracture Structures

Book ISBN: 978-1-56990-557-9

eBook ISBN: 978-1-56990-558-6

For further information and order see

www.hanserpublications.com (in the Americas)

www.hanser-fachbuch.de (outside the Americas)

Preface

Polymers are important materials in many fields of daily life, from household, medicine, agriculture, and automotive industry products, up to microelectronics and space research. The morphology of polymers provides and controls the physical, chemical, and other properties of technical relevance. Therefore, analysis and control of the morphology of polymers is a crucial precondition to material development, to improve properties in general and to better fit specific properties to defined applications.

In the last few decades, the amount of interest in polymeric systems has gradually shifted from the micron-scale to the nanometer-scale region. As a consequence of the trend toward producing more nanostructured polymers and miniaturizing components (microsystems), a better understanding of the hierarchical structure of polymers is needed. In general, knowledge of the property-determining structures and microprocesses or mechanisms is a necessary precondition for exploiting the full potential of polymeric materials and is key in successfully developing new polymers and improving the properties of polymers already in use. This Atlas will help scientists and engineers to understand the morphology of polymers and, therefore, to understand their properties better.

The detailed investigation of the complex hierarchical structures of many polymers requires the use of specialized techniques. Electron microscopy and atomic force microscopy have both developed into powerful tools in the field of polymer science. By using different techniques, morphological details can be detected at length scales from the visible (0.1 mm) down to the atomic level (about 0.1 nm). Additionally, the influence of several parameters, such as temperature, environment, and mechanical stresses, can be investigated together with the morphology of the material. In particular, under mechanical loading, the influence of the local morphology on the mechanical effects that occur at the nano- and microscopic level can be examined. Therefore, electron microscopy and atomic force microscopy directly contribute to a better understanding of structure-property correlations in polymers.

This book reviews the research results of academia and industry with a comprehensive overview of the morphology of all groups of polymers. The different levels of morphology, that is, the hierarchical structure of polymers, are illustrated with micrographs from all of the different microscopic techniques with magnifications from the millimeter down to the subnanometer scale. In addition, changes in morphology during and after mechanical loading up to fracture structures are presented together with illustrations of the nano/micromechanical and failure mechanisms. The reader will find a compact and understandable description and illustration of the structural or morphological variety of polymers with a focus on the morphological details, which are relevant for the application properties of the polymers. The micrographs and explanations allow correlations between the morphology and properties of the polymers and help readers to better understand the ultimate properties. The aim of this book is to give guidelines for polymer researchers, chemists, chemical engineers, and material scientists in institutions and industry for understanding the principles of morphology formation and for improving

properties, in particular mechanical properties. Finally, the book will also be helpful for students of polymer physics, chemistry, and engineering, as well as for those researchers interested in the microscopic and nanoscopic world of polymers.

After an introductory chapter in Part I of the Atlas, with an overview of the molecular and supermolecular structures (morphology) and the mechanical behavior of polymers, Chapter 2 offers a summary of the main techniques and methods used to investigate the nanostructure and morphology as well as the nano- and micromechanical processes and mechanisms. It describes briefly the wide variety of preparation methods and the different microscopic techniques of electron microscopy and atomic force microscopy used in morphological investigations, accompanied by representative micrographs. In particular, contrast formation in the different microscopes is discussed to help the reader to interpret the micrographs of the many polymers. Chapter 3 discusses several factors of sample preparation as well as investigation technique that can influence the appearance of micrographs or lead to false interpretations.

The subsequent nine chapters of Part II form the main part of the Atlas, with the presentation of micrographs of the different groups of polymers, including amorphous and crystalline polymers, block copolymers, blends and rubber-toughened polymers, particle- and fiber-reinforced composites, biopolymers and biomedical polymers, nanofibers, and special polymer forms. Each of these chapters starts in the first section with a general overview of the particular polymer group; the following sections show in detail representative micrographs from different microscopic techniques with short descriptions, illustrating the characteristic features and also the variety of structures and morphologies of the polymers and showing the influence of the preparation method. In addition to the legend for each micrograph, in some cases micrographs are grouped and compared in one figure with extended information. In all cases, a clear identification of magnification with a scale bar and, if necessary, the direction of mechanical loading are indicated. Next to the typical morphologies, examples of deformation and fracture structures together with the relevant deformation mechanisms and the most commonly occurring defects and failures are highlighted as well. Each chapter closes with a list of relevant references.

In Part III are some tables to help the reader quickly find the figures of the different polymers illustrated in Part II and find micrographs with characteristic morphological details and characteristic deformation and fracture structures. In addition, some morphological terms have a culinary or natural background.

This book presents lots of illustrating micrographs that result from all of the direct imaging methods of optical, electron, and atomic force microscopy. It contains knowledge and experiences developed over more than four decades in different working groups in academia, universities, applied research institutes, and the polymer industry. For many of the microscopic investigations and micrographs I thank my former coworkers in Halle, Schkopau, and Merseburg, Germany, in particular DI (FH) Irene Naumann, DI (FH) Helga Steinbach, Dr. Katerina Morawietz, Ingeburg Schülke, DI (FH) Sylvia Goerlitz, Cornelia Becker (†), Dipl.-Phys. Werner Lebek, Dipl.-Phys. Volker Seydewitz, DI Stefanie Scholtyssek, Dr. Reinhold Godehardt, Dr. Ashraf Sh. Asran, Dr. Sven Henning (now Fraunhofer Institute of Materials Mechanics in Halle), Dr. Rameshwar Adhikari (now Kathmandu, Nepal),

Prof. Dr. Gyeong-Man Kim (now South Korea), Prof. Dr. Roland Weidisch (†), and many diploma and Ph.D. students. Valuable contributions with micrographs of several polymers came from Dr. František Lednicky, Institute of Macromolecular Chemistry of the Czech Academy of Sciences in Prague. For special micrographs I want to thank many friends and colleagues, including Prof. Dr. Volker Abetz, Geesthacht, Prof. Dr. Andrzej Bledzi, Kassel, Prof. Dr. Stoyko Fakirov, Auckland, New Zealand, Prof. Dr. Hans-Peter Fink, Potsdam-Golm, Prof. Dr. Klaus Friedrich, Kaiserslautern, Prof. Dr. Andrzej Galeski, Lodz, Poland, Prof. Dr. Jozsef Karger-Kocsis, Budapest, Ungarn, Prof. Dr. Lacayo Pineda, Hannover, Dr. Arthur Bobovitch, Beer-Sheva, Israel, Dr. Ralf Lach, Merseburg, Ing. Claudia Mayrhofer, Graz, Austria, Dr. Christopher Plummer, Lausanne, Switzerland, and Dr. Helge Steininger, Ludwigshafen. In particular I have to thank DI Wofgang Schurz and DI Sven Borreck (†) for transforming many of the micrographs into a digital form, for image processing, and for technical editing of figures.

Many examples of polymers with representative micrographs together with a description of the nano- and micromechanical properties are from the first publication in this field by G. H. Michler, "Kunststoff-Mikromechanik: Morphology, Deformations- und Bruchmechanismen," Hanser, 1992, and from the book "Nano- and Micromechanics of Polymers: Structure Modification and Improvement of Properties," Hanser, 2012, together with my friend Francisco Jose Baltá-Calleja, Madrid, whom I also thank for improvements of the manuscript. For helpful discussions over many years, I thank Prof. Dr. Dr. h.c. Hans-Henning Kausch, Lausanne, Switzerland, and Prof. Dr. Wolfgang Grellmann, Merseburg, Germany.

Finally, I thank the Carl Hanser Verlag for the cooperation and the careful realization of the book project.

Halle (Saale), September 2015 *Goerg Hannes Michler*

Contents

I

Part I – Introduction

CHAPTER 1

Overview

1.1 Aim of the Atlas

Polymeric materials show a very broad variety in structure and morphology and possess very different specific properties. The production of the first polymers used as manufacturing materials started over 100 years ago with the realization of phenol resins by L.H. Baekeland. The first polymer plant in the world in Erkner near Berlin began in 1910 with the production of such resins well-known as Bakelite. In the beginning of the 20th century, these resins conquered a big market, particularly in electrical applications and due to increased substitution for classic materials such as ivory, wood, metal, glass, or porcelain. However, soon it was found that polymeric materials are not only copies or substitutes, but possess specific properties that gradually opened new applications in fields in which they were superior to conventional materials. A deeper knowledge of the structure of these materials started in 1926 with the idea of H. Staudinger, and that is that they (polymeric materials) consist of large macromolecules that are chemical linkages of many small monomer molecules that are arranged like a string of beads. The synthetic production led to the German word "Kunststoffe" for these materials. The English words "polymers" and "plastics" are related to their composition and basic properties. Up to now, there has been a worldwide increasing production of all types of polymers, thermoplastics, resins, and rubbers, with annual average growth rates currently about 5–10% with an estimated consumption of over 300 million tons by 2015. A steady growth in polymer production is also expected in the future [1].

The main arguments to use polymeric materials are

- easy processability and moldability, even of difficult forms,
- low production costs (better energy balance per volume than for many other materials, such as steel or aluminum),
- light weight and advantageous strength/weight ratio, and
- easy modification with other polymers and inorganic components.

Because of these specific and other properties, polymers are used in nearly all sectors of industry, in agriculture and medicine, in everyday household articles, and in space research. Because of the broad variety of polymeric structures, they can be precisely adapted to particular applications, and the variedness of polymers is not surpassed by any other class of materials. So we can say that polymers are everywhere and that they are the materials of the 21st century—we can speak of a dawning "age of polymers."

Currently more than 80% of all thermoplastic materials are based on the so-called *mass polymers* or *commodities*, for example, polyethylenes, polypropylenes, polystyrene, and poly(vinyl chloride). Compared to these, the contribution of the so-called *engineering polymers* is relatively small: poly(methyl methacrylate), polyamides, and polycarbonates together account for about 4%. High-performance plastics such as poly(phenylene sulfide), poly(ether ether ketone), or fluoro-

polymers hold a negligible share of the market. Additional important groups of polymers are rubbers and thermosets or resins. The renaissance of mass polymers is due to improved polymerization routes, controlled molecular weight and macromolecular design, better macromolecular regularity, modifications of the macromolecular architecture and composition, as well as blending of different polymers and modification with inorganic fillers and fibers. At the same time, the interest has shifted to smaller details, from the former micrometer level to the now increasingly more important nanometer level. This increasing tendency for structural modifications has also pushed polymer research to achieve accurate correlations between synthesis or polymerization, molecular structure, morphology, and properties as a topic of materials science. Figure I.1 illustrates correlations between molecular (or chemical) structure, supermolecular structure or morphology (which depends on the polymerization route as well as on processing conditions), and mechanical properties (which also depend strongly on loading conditions). The micro- and nanomechanical processes under load are of central importance and provide the bridge between structure/morphology and mechanical properties. Mechanical properties are also of importance for applications where other properties (such as optical, electrical, magnetic, biological, and medical) are of interest. If there is a mechanical failure, such as a premature fracture of the polymeric material, these other properties cannot be realized. Similar correlations between structure/morphology, micromechanisms, and ultimate behavior also exist for other properties of interest.

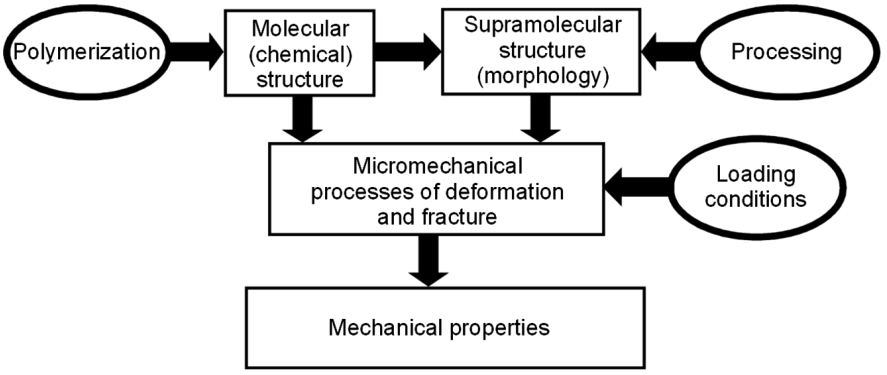

Figure I.1 Scheme of correlations between polymerization, molecular structure, morphology, processing conditions, and micro- or nanomechanical mechanisms of deformation and fracture depending on loading conditions, all of which determine the ultimate mechanical properties

To determine in detail the morphology of polymers and to gain a better understanding of structure-property correlations, electron microscopy, and atomic force microscopy are widely used techniques [2]. With the shift of interest to smaller and smaller structural details, these microscopic techniques are becoming more and more important. The recent increased availability of high-resolution electron microscopy and atomic force microscopy (AFM) is now making it possible to view macromolecular arrangements, and this should lead to further advancements in our understanding of the forms and structures of all types of polymeric materials. An additional trend is to reveal not only structural details but also changes in morphology under the action of influencing parameters, such as physical and thermal aging, outdoor weathering, effects of chemical treatment, and mechanical loading. Many such changes can be studied directly with microscopic methods, in particular with the so-called *in situ microscopy*. The influence of mechanical

loading on changes in the structure and morphology of polymers, and their nano- and micromechanical properties and mechanisms, can be revealed by microscopic methods with an otherwise unattainable accuracy [3, 4].

From the huge variety of macromolecular and supermolecular structures, not all of them are of equal relevance for property improvements. For the example of mechanical properties, only a few structures determine the mechanical behavior of the polymer, and these are called "property-determining structures" [3]. Detailed knowledge of these structures and the underlying nano- and micromechanical mechanisms enable criteria to be defined for the modification and production of polymers with specifically improved or new properties. This way is known as the "microstructural construction of polymers" [4, 5]. In addition, an improved knowledge of structure-property correlations is helpful in deciding whether newly synthesized polymeric materials possess a morphology that offers the potential for a new material. However, to instead design new macromolecules with different chemical compositions, it is easier and cheaper to modify known macromolecules or polymers with the knowledge of detailed correlations between structure/morphology and properties. On the other hand, materials in nature with an outstanding combination of different properties (such as wood, mother of pearl, and human bone) act increasingly as models for designing a hierarchical morphology of polymers. Special biocompatible and biodegradable polymers are materials for regenerative medicine (tissue engineering).

The broadness of properties and applications of polymers is based on the chemical structure (constitution, configuration, and conformation) and morphology. But materials of the same chemical structure can be modified in such a manner that they reveal different morphologies and properties. On the other hand, polymers of different chemical structures can possess a similar morphology with similarities in properties and behavior. An overview of the broad variety of morphology of polymers helps to better understand the properties and possible structural modifications of polymers. It is a basic human requirement to make a picture of things we want to understand. There is a proverb that is often used by microscopists about the value of their work: "A picture is worth a thousand words." In this sense, this atlas will support a better understanding of the morphology of polymers and its influence on properties, particularly mechanical behavior. For instance, knowledge of the specific structure of one polymer with a good strength or toughness can be helpful in modifying the structure of another polymer to realize similar good properties. Moreover, the collection of morphologies in this atlas will promote polymer research to learn more on known polymers and to find ways of creating new materials.

This book, the *Polymer Atlas*, presents a collection of micrographs of the morphology of a broad variety of polymers. Additionally, changes in morphology under mechanical loading and the illustration of deformation processes and fracture surfaces are shown in detail. Features of the *Polymer Atlas* are as follows:

- Provides an up-to-date collection of micrographs from the millimeter scale down to the micrometer and nanometer scale from all types of microscopes (optical microscope, scanning, and transmission electron microscopes (SEM and TEM), environmental scanning electron microscope, high-voltage electron microscope, atomic force microscope)

- Includes all groups of polymers of practical importance and scientific interest with representative examples
- Addresses representative micrographs of morphology of polymers and explains details
- Provides micrographs of deformation structures and fracture details
- Includes information on preparation and methods of investigation of the morphology

In this introductory section of Part I, Sections 1.2 and 1.3 present basic connections between chemical structure and morphology with an overview of the hierarchical structure of polymers. Section 1.4 gives a brief characterization of the mechanical behavior of polymers. For a better understanding of the micrographs, a short description of the different microscopic investigation techniques and the sample preparation methods is presented in Chapter 2 of this part (Sections 2.1 and 2.2). Techniques and methods to study deformation structures, micromechanical mechanisms, and fracture details are the content of Section 2.3. Possible influences on the morphology due to sample preparation or microscopic investigation are considered in more detail in Chapter 3.

The main Part II of the *Polymer Atlas* contains a rich collection of micrographs of all of the interesting groups of polymers in the following chapters:

1. Amorphous polymers, including homopolymers such as polystyrene (PS), poly(methyl methacrylate) (PMMA), polycarbonate (PC), poly(vinyl chloride) (PVC), and copolymers such as styrene acrylonitrile copolymer (SAN) and cyclic olefin copolymer (COC)
2. Semicrystalline polymers with the polyethylenes, polypropylenes, polyamides, and others
3. Block copolymers, including two-, three-, and multiblock copolymers
4. Polymer blends, including blends of amorphous polymers, amorphous and semicrystalline polymers, semicrystalline polymers, and rubber blends
5. Rubber-toughened polymers with an amorphous matrix and semicrystalline polymer matrix
6. Composites with micro- and nanosized particles (commercial composites and nanocomposites)
7. Fiber-reinforced polymers with inorganic, organic, and polymer fibers
8. Biobased, biodegradable, and biomedical polymers
9. Special processing forms, such as hot compacted polymers, coextruded multilayer polymers, electrospun nanofibers, and polymer foams

The description of each polymer group starts with an overview of the basic structural features and properties and representative references. The micrographs in the following sections are arranged in such a manner that the different polymers of this group are shown at first with typical, characteristic structures and with the variation in morphology and secondly, with structural changes due to loading, with typical deformation structures and fracture details. To each micrograph a short description is added of the characteristics of the morphology, of the preparation technique of the material, how the sample was prepared, and what observation

technique (with what microscope) was conducted. Representative references for additional information are included. The reference lists for the micrographs are listed at the end of each chapter. Most of the micrographs come from working institutions of the author in academies, the chemical industry, universities, and research institutions. Additional micrographs are contributed by friends and colleagues from industry and research institutions worldwide. In this case, sources and typical publications are mentioned.

It is easy to find special polymers in this atlas because of the classification into the nine groups of different polymers. To also make it easier for the reader to find different polymers, special morphological types, and details, as well as characteristic deformation and fracture structures, several tables are introduced in the special Part III. An index is at the end of the atlas.

1.2 Molecular Structures

Polymers consist of macromolecules that have a large number of either identical or different monomer units, which are connected by covalent bonds. The number of monomers usually varies between 10^3 and 10^5, yielding molecular weights of macromolecules (product of the number N and molecular weights of the monomers) ranging between 10^4 and more than 10^6. The chemical structure, the arrangement of the monomers, and the shape of the macromolecular chains are described by three parameters, the “three Cs”: constitution, configuration, and conformation.

1.2.1 Constitution

Constitution is defined by the chemical nature and composition of the monomers. The simplest case is an arrangement of identical ethylene monomers, C_2H_4, in a polyethylene macromolecule: $-(C_2H_4)_n-$. Homopolymers contain only one type of monomer in the chain. Copolymers, block copolymers, graft polymers, or terpolymers consist of two or more different kinds of monomers.

1.2.2 Configuration

Asymmetric monomers can be arranged in different ways along the macromolecular chains, i.e., in different configurations; see Fig. I.2. Tacticity describes the arrangement of monomers with substituents or side groups (Fig. I.2):

- Atactic polymers show a random arrangement of monomers along the chain.
- Syndiotactic polymers exhibit an alternating arrangement of side groups.
- Isotactic polymers possess identically positioned monomers.

Side groups or branching along the main chain define another type of homopolymer configuration (Fig. I.3). Short-chain branches can be distributed statistically, comb-like, or concentrated locally, for example, at the ends of the macromolecules or on shorter macromolecules (with lower molecular weight). Short- and long-chain branches can be combined and macromolecules cross-linked by side chains to form a three-dimensional network. Networks with higher cross-linking density (thermosets, resins) cannot melt without degradation.

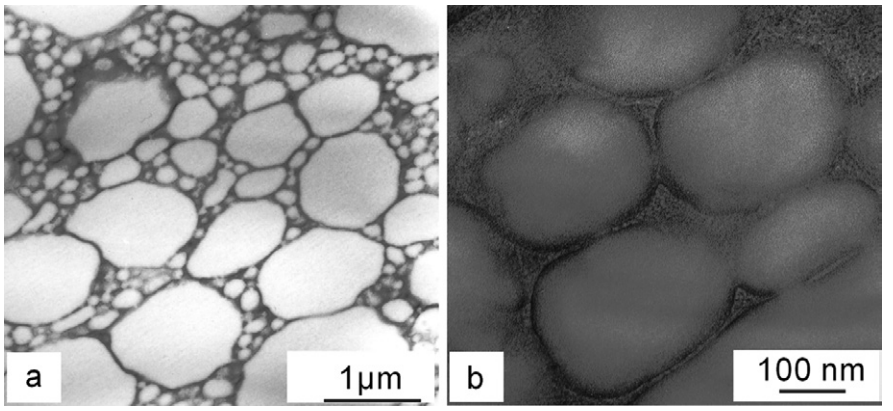

Figure I.12 Network morphology of a PS/PE (75:25) blend with a PE network containing embedded PS particles:
(a) smaller magnification of a dense network of PE with larger and smaller PS particles;
(b) larger magnification of the PE network with visible lamellar structure around PS particles; stained UDS, TEM

In general, the morphology of a blend of different polymers is determined by the phase distribution of the components (usually distribution of the minor component in the major one) and the morphology of each component (e.g., amorphous, semicrystalline). It is more complex when more than two components exist. A three-phase morphology appears in Fig. I.11 with an amorphous phase of VLDPE and crystalline and amorphous phases of HDPE, and an example with five-phase morphology is shown in PA/ABS blends in Fig. 4.5 in Part II. Apart from such disperse systems, with a dispersed distribution of one (usually the minor) component in the other one, network systems with a network of the minor component embedding particles of the major component also exist. A network morphology with about 0.1–1 µm PS particles (major component) in a PE network (minor component) is presented in Fig. I.12. The classic example of a network morphology is toughened PVC with very thin rubbery layers (often EVA) wrapped around the primary particles of PVC about 0.5–1 µm in diameter (see Fig. 5.5). Between network structures and disperse structures, all sorts of transitional structures may appear (see examples in Chapters 4 and 5 in Part II).

Another class of polymer blends form the so-called rubber-toughened polymers because of their good mechanical properties and particularly toughness. In these polymers, usually particles of a rubbery, elastomeric polymer are distributed in a brittle or stiff matrix, initiating under load special energy-absorbing processes (e.g., crazes or shear bands; see Chapter 5 in Part II).

Special polymer blends can be realized using the coextrusion technique. Using two or more extruders, the individual melt streams are put together in a multilayered arrangement, and polymer systems of two up to five clearly visible layers can be produced. Using the special multilayer coextrusion technique, polymer systems of two or three different polymers with a parallel arrangement of up to several thousands of very thin layers are possible; see Section 9.3 in Part II.

1.3.4 Composites

Composites are composed of a polymeric matrix that contains inorganic reinforcement components (particles or fibers). The matrix material surrounds and supports the reinforcement materials by maintaining their relative positions. The reinforcements are embedded and arranged in specific internal configurations to obtain mechanical or other properties tailored to specific applications.

Depending on the reinforcing material, composites are divided into two main categories, normally referred to as particle-reinforced polymer composites and fiber-reinforced polymer composites.

In particle-reinforced polymer composites, the particles used to reinforce polymers include ceramics and glasses (small mineral particles such as Al_2O_3, $CaCO_3$, and talc), metal particles (for example, Fe, Ag), or also organic particles of wood, rice hulls, or starch. In composites, particle diameters vary from some micrometers up to several tens of micrometers; in nanocomposites the particles are in the range of some hundreds of nanometers down to 10 nm. Broad diameter distributions enable high filler contents because the spaces between the large particles are filled with smaller ones. The shape of the particles can be irregular (as in chalk), layered (as in kaolin), or spherical (as in glass beads, Fig. I.13). Most mineral particles are typically used to increase the modulus of the matrix, to increase wear and abrasion resistance and surface hardness, to improve performance at elevated temperatures, to reduce friction and shrinkage, and to decrease the permeability of the matrix. Metal particles are mainly used to improve the electrical conductivities of most insulating polymer matrices.

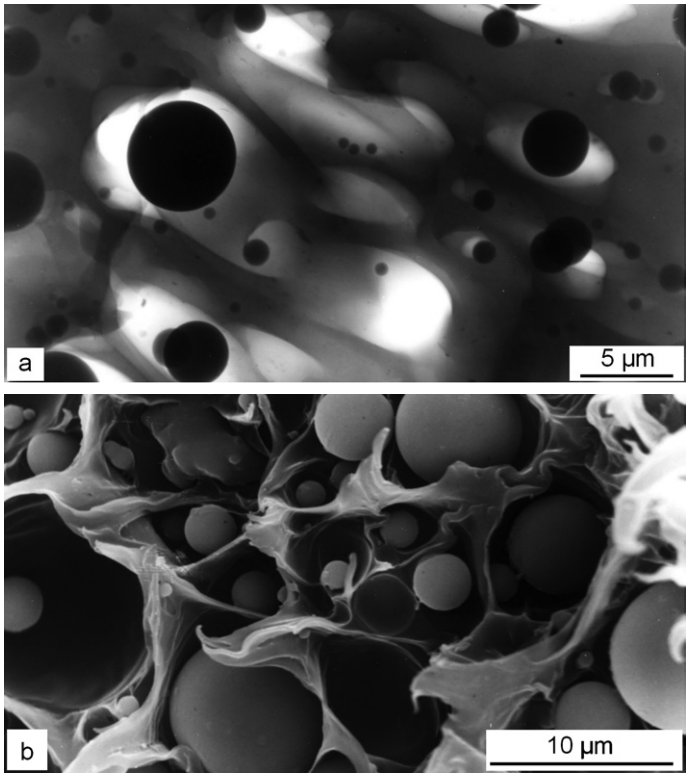

Figure I.13 Particle-filled composite with a broad size distribution of spherical glass beads:

(a) deformed in HEM with debonding and void formation around the beads;

(b) fracture surface in SEM with plastic deformation of matrix strands between voids

The mechanical properties of particle-filled polymers are influenced by the stiffness of the particles, the diameter, and the shape, as well as by the adhesion between the particles and the polymer matrix (interfacial strength). In the case of good interfacial strength, the well-bonded particles contribute to stiffness and strength enhancement of the composite. Debonding usually decreases stiffness and strength, but in some cases it can contribute to enhanced toughness. Under load, stress concentration at the poles of the particles initiates a debonding process

at both sides of the particles in the direction parallel to the applied stress. This is seen in a composite with a broad distribution of spherical glass beads, uniformly dispersed in the matrix in Fig. I.13(a) in an in situ deformation test. The larger particles easily debond under external load, which leads to the formation of large microvoids around the particles. Here, the matrix strands between the elongated voids around the beads are plastically stretched, and these stretched matrix regions are visible on fracture surfaces as fibrils in a typical dimple structure; see Fig. I.13(b) in an SEM micrograph. The competition between debonding, size of voids, interparticle distance, and ductility of the matrix polymer determines the ultimate mechanical properties.

Fiber-reinforced polymer composites can contain short, discontinuous fibers (usually in thermoplastics; see Fig. I.14) or long, continuous fibers in thermoset resins. Fibers can vary from the usual glass fibers with thicknesses of some tens of micrometers up to nanofibers or carbon nanotubes (single-walled or multiwalled, SWCNT or MWCNT) about 10 nm thick. The properties of fiber-reinforced composites depend on thickness, length, and volume content of the fibers, as well as on adhesion (interfacial strength) and matrix properties.

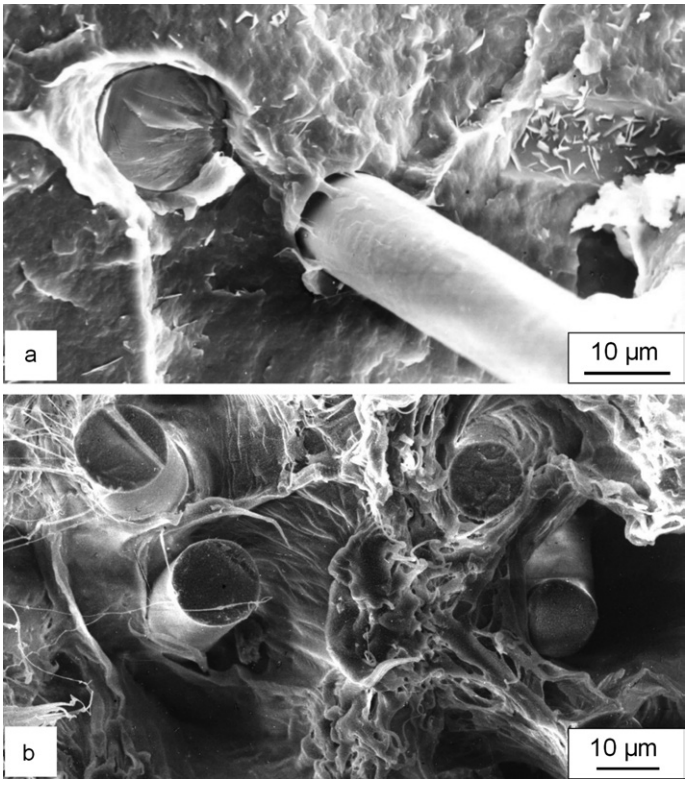

Figure I.14 Glass-fiber-reinforced PP composites in fracture surfaces in SEM:

(a) with poor phase adhesion;

(b) with good adhesion

Composites with natural particles or fibers such as wood, bamboo, sisal, jute, wheat straw, banana, or coconut form another group of polymer composites. They are considered with other biopolymers in Section 8.2 in Part II. The so-called *hot-compacted polymers* can be considered as special fiber composites. The idea behind this is to make high-strength compositions starting from highly oriented anisotropic fibers or tapes of a single polymer, which are connected to woven mats and compacted with the technology of "hot compaction" (see Section 9.2 in Part II).

1.3.5 Additional Morphologies

In addition to the above-mentioned commercial polymer groups, some polymers with special morphologies and properties exist. The above-mentioned hot compacted self-reinforced polymers and the coextrusion multilayered polymers with a parallel arrangement of up to many thousands of layers only a few nanometer thick layers are two examples (see Sections 9.2 and 9.3 in Part II). Another interesting group are nanofibers produced by electrospinning. They possess thicknesses of some hundreds of nanometers and outstanding properties for technical and particularly medical applications; see Section 9.4. Foams with a high content of micro- or nanovoids are important for insulating and filtering applications (Section 9.5).

There are some interesting types of structure or morphology, which are named after culinary products, like shish kebab structures (from schaschlik) in PE and PP or salami particles in HIPS. They are listed in Part III in Table 4.

1.4 Mechanical Behavior

1.4.1 Types of Deformation

The term "mechanical behavior" refers to the reaction of a material under mechanical loading. When a force acts on a body, the result is a deformation or a fracture, depending on the material and the type of loading (tension, bending, compression) and loading condition (load rate, temperature, and so on). The great variety in mechanical properties of polymers is illustrated in Figure I.15 by typical stress-strain curves. The range of mechanical properties spans from brittle fracture to highly ductile behavior and rubber elasticity. There are many quantities that permit the characterization of the macroscopic mechanical performance of materials. Besides quantities derived from stress-strain tests, such as modulus of elasticity (Young's modulus), yield stress, fracture stress, strain at break, and others, there are also related quantities from bending or compression tests and from cyclic loading. Fracture toughness as a measure of energy absorption during loading up to fracture can be measured by the area below the stress-strain curve or is determined by methods of fracture mechanics.

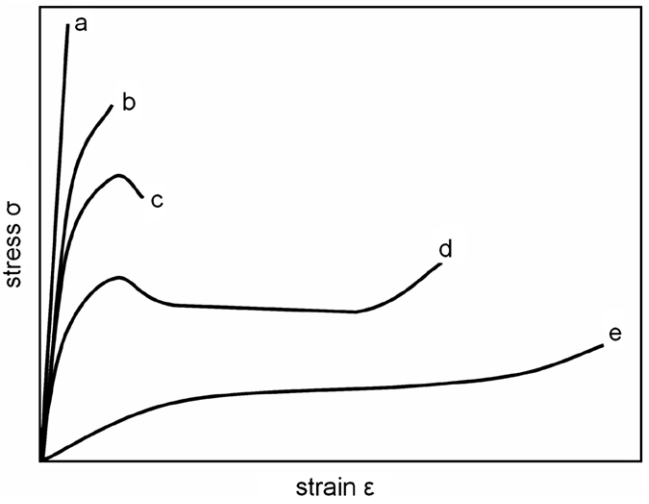

Figure I.15 Idealized, typical stress-strain curves of different polymers:

(a) highly oriented fibers of high modulus and strength, linear increase in load (examples are fibers of PE, PP and PA);

(b) (semi)brittle fracture, linear increase of load up to a small deviation at high strength (e.g., PS, PMMA);

(c) necking with ductile behavior, load increase up to a yield point with load decrease, fracture above 10% (e.g., PVC, PC);

(d) cold drawing, increase of load up to a yield point, load decrease, large strain with strain hardening, fracture at large strain up to about 100% (examples PE and PP);

(e) homogeneous deformation, rubber elasticity, continuous load increase with very high tensile strains at break (e.g., natural, synthetic rubber)

CHAPTER 3

Influences of Techniques and Methods on Micrographs

As has already been shown, the method of preparation and the investigation technique for polymers can influence the appearance of morphology of the particular polymer. In addition, one must consider whether varying the preparation methods and microscopic techniques can improve or even deteriorate the visibility of structural details. Some examples of the practical importance of sample preparation and of microscopic technique that can strongly influence the visibility of structures in the micrographs are described in the following sections.

3.1 Influence of Sample Preparation

3.1.1 Influence of Fracture Processes

As mentioned before, fracture surfaces can reveal the morphology of broken material. However, structures from the fracture process also often modify the real morphology of the sample. Surfaces from *ductile fracture* show plastic deformation structures. Therefore, surfaces from brittle fractures should usually be used, but also here fracture-characteristic features can mark the surface. An example is shown in Fig. I.37 with a parabolic structure on a fracture surface not presenting a morphological detail of the sample but a secondary crack, initiating from a defect particle. On the other hand, *brittle fracture surfaces* also contain brittle fracture edges from the polymeric material, often independent of the polymer morphology. In some cases, the method of "soft-matrix fracture" can be helpful (see Section 2.2.2, Fig. I.36).

3.1.2 Influence of Section Thickness

Ultrathin sections are somewhat difficult to prepare and reveal only a thin layer of the material, which gives more two-dimensional information on the morphology than a three-dimensional one. Thicker semithin sections often reveal much better the size and shape of particles in polymer blends, rubber-toughened polymers, and others. Additionally, semithin sections represent "bulk-like" properties better than do ultrathin sections if they contain a "representative volume" of the material.

Using TEM with accelerating voltages of 100–200 kV, specimen thicknesses of less than 100 nm are required. Thicker sections of up to about 500 nm thick produce a lot of inelastically scattered electrons, which reduce contrast and resolution. Using electron energy-loss spectroscopy (EELS) in energy-filtered TEM (EFTEM), all inelastically scattered electrons can be removed so that only the unscattered electrons of the primary beam and the elastically scattered electrons that pass through the objective aperture contribute to the image. Such "zero-loss" imaging avoids chromatic aberration, enhances the contrast, and improves the resolution. This is demonstrated in Fig. I.57 by a stained 400 nm thick semithin section of an ABS (acrylonitrile-butadiene-styrene) polymer investigated in EFTEM with a

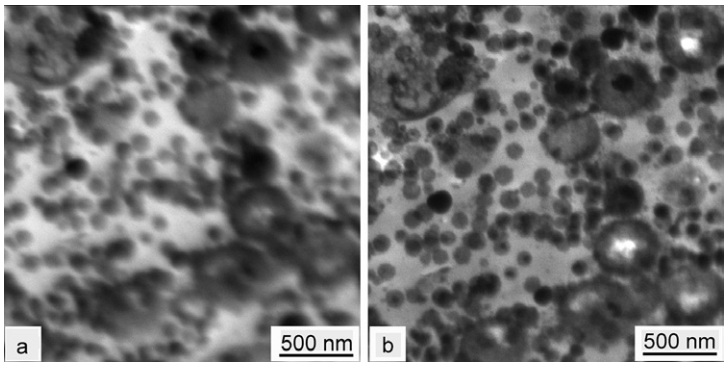

Figure I.57 Improvement of contrast and resolution of a stained 400 nm thick ABS section produced by zero-loss filtering in an EFTEM (b) compared to global mode imaging (a)

Omega filter used in the global mode (a) and of the same area by zero-loss filtering (b) [1, 2].

A main goal of HEM working at a voltage of 1 MV or even higher is the possibility of using specimen thicknesses that are some three to ten times larger than possible with a conventional TEM (see Section 2.2.1). A comparison of ultrathin sections with semithin sections demonstrates the advantage of using thicker sections. Figure I.58 schematically shows a particle-filled polymer matrix where ultrathin sections only contain small parts of the particles, and where semithin sections contain undamaged particles in their typical surroundings. Figure I.59 compares the visibility of the size and shape of the rubber particles (so-called salami particles) in HIPS. In ultrathin sections, only small cross sections of particles are visible, which are usually smaller than the real diameter; this effect is known as the "tomato salad problem." In addition, the particles are deformed due to compression during sectioning (see Figs. I.44 and I.45). Only thicker sections of 1 μm and 4 μm thickness show the true shape and size of the larger particles without deterioration. The true particle diameter of on average 1 μm is visible only in the thickest section of 4 μm; see Fig. I.59 (bottom). The measured average size using ultrathin sections is only 50% of this value. In general, if particles are larger than the section thickness, the measured frequency distribution of particle size is shifted to smaller diameters [2, 3].

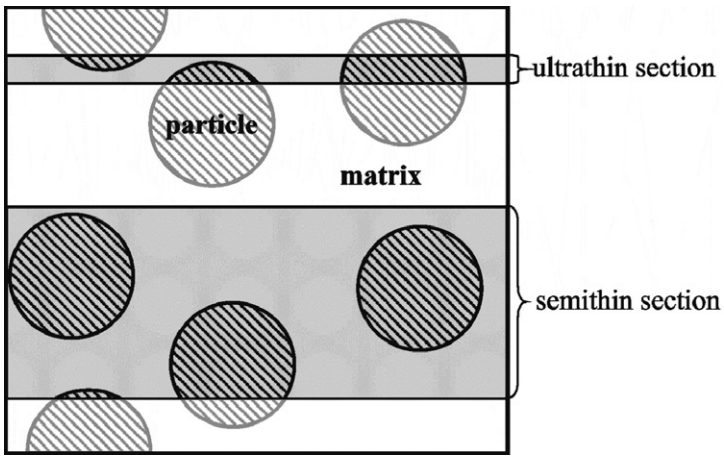

Figure I.58 Schematic illustration showing the effect that ultrathin sections include only small parts of particles in a matrix, whereas semithin sections contain a "representative volume"

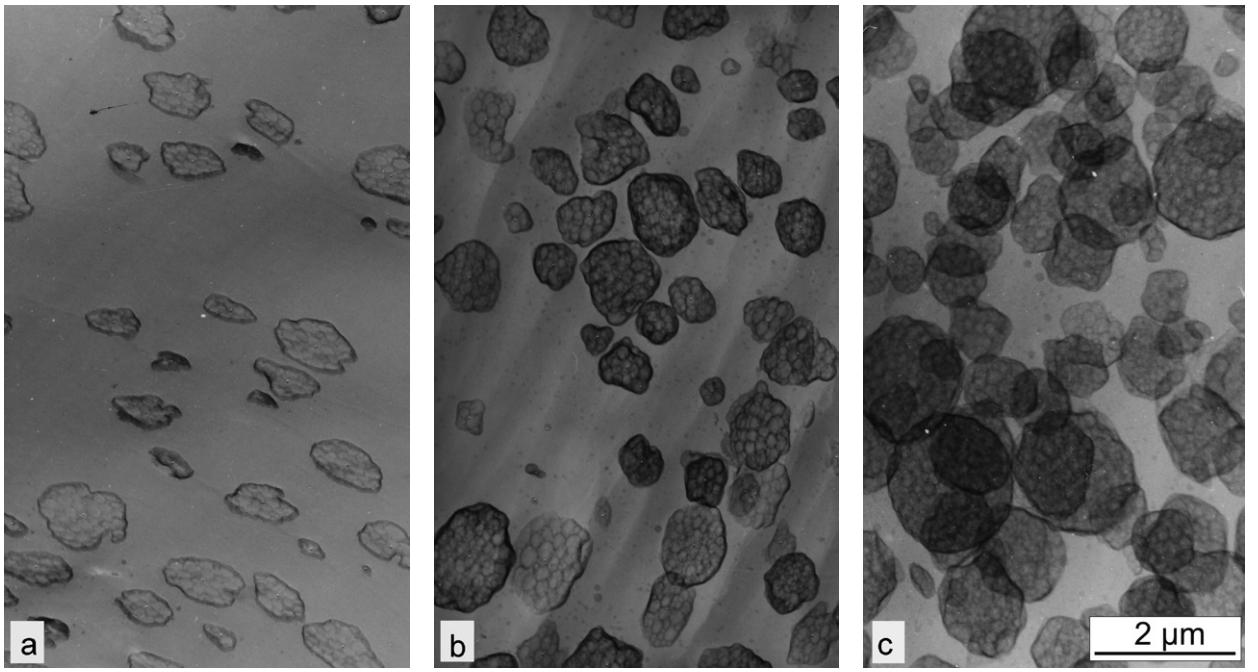

Figure I.59 (top) Salami particles in HIPS visible in sections of different thickness:
(a) 0.1 µm;
(b) 1 µm;
(c) 4 µm
(rubber particles selectively stained, HEM)

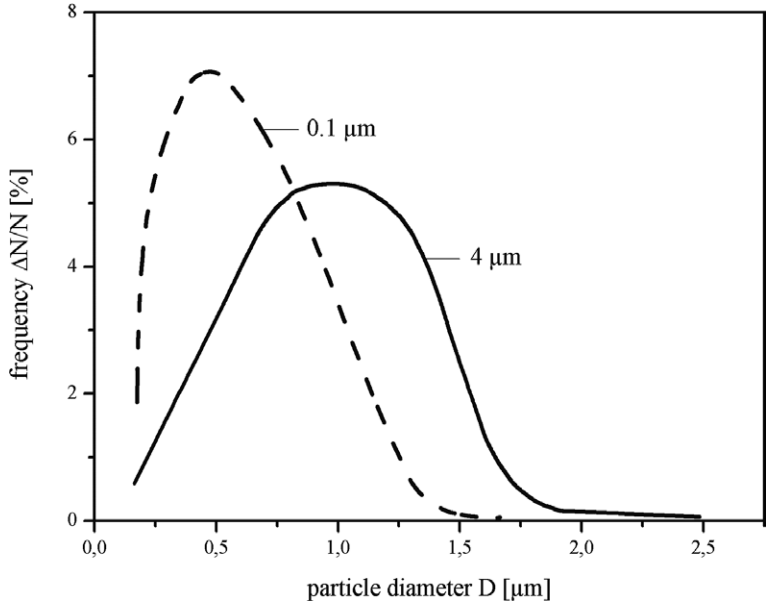

Figure I.59 (bottom) Frequency distributions of rubber particles in sections of different thickness of HIPS (see Fig. I.58, top): 0.1 µm ultrathin sections show only smaller cross sections of the particles, whereas the 4 µm thick semithin sections reveal the true average particle diameter

II

Part II – Groups of Polymers

CHAPTER 1

Amorphous Polymers

1.1 Main Characteristics

1.1.1 Structure and Morphology

Polymers of this group have their "amorphous" structure in common. In contrast to the usual definition of amorphous, meaning structureless, many amorphous polymers reveal a more or less detectable microstructure, from weak domain-like or globular structures up to a pronounced morphology. Therefore, a second definition is often used that amorphous polymers do not exhibit any crystalline structure in X-ray or electron scattering experiments. According to this definition, very different materials belong to the family of amorphous polymers:

- the amorphous thermoplastics, including glassy, brittle polymers (such as PS and PMMA) and ductile polymers (such as PVC and PC);
- the statistical copolymers, terpolymers, and graft polymers (such as SAN and COC);
- block copolymers containing amorphous polymer blocks;
- polymer blends and rubber-toughened polymers with amorphous components;
- resins, such as polyesters and epoxies;
- particle-filled and fiber-reinforced composites with an amorphous polymer matrix.

The amorphous brittle and ductile homopolymers are illustrated in Section 1.2 and the amorphous copolymers in Section 1.3. The other polymers form separate groups and are illustrated in Chapter 3 (block copolymers), Chapter 4 (polymer blends), Chapter 5 (rubber-toughened polymers), Chapter 6 (particle-filled micro- and nanocomposites), and Chapter 7 (fiber-reinforced polymers).

The shape or form of the macromolecules of amorphous polymers (the conformation; see Section I.1 in Part I) is described by the *random* or *statistical coil model* with a statistical arrangement of the successive monomer segments [1]. The macromolecules form coils in the solid state with diameters corresponding to the coils of macromolecules in a highly diluted theta-solvent. The diameter of the coils is proportional to $\sqrt{M_w}$ and usually ranges between 10 and 30 nm; for instance, a PS macromolecule with a molecular weight of $M_w = 2 \cdot 10^5$ reaches a coil diameter of about 30 nm [2]. The density of an individual random coil is in the range of 0.01 g/cm^3. Since the density of an amorphous polymer is about 1 g/cm^3, this means that roughly several hundred macromolecular segments of neighboring macromolecules must exist in the same volume within the polymer. These result in a strong interpenetration and in the formation of lots of topological, physical links: the *entanglements*. The entanglements act as physical connecting points and determine to a high degree the stress transfer between the macromolecules and the strength of a polymeric body. Parameters include the diameter of the macromolecular coil, the entanglement distance d, and the molecular weight of the macromolecular segments between the entanglements (M_e); see Fig. 1.1.

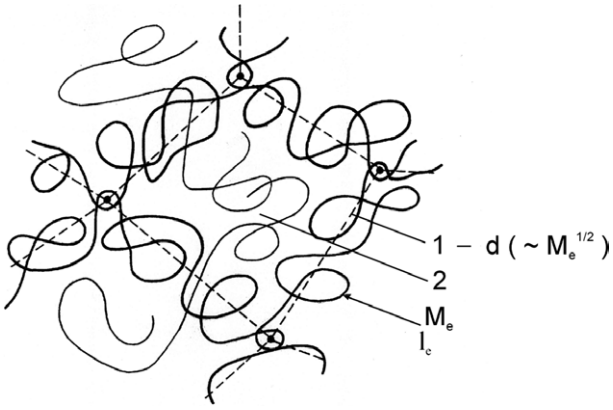

Figure 1.1 Entanglements in an amorphous polymer, connected to an entanglement network; M_e and l_e are the molecular weight and the length of the segments between entanglements, respectively; d is the distance between entanglements; 1 marks the entanglement network and 2 the meshes of the network

The entanglement points between the macromolecules can be connected to form a network with meshes and a mesh diameter D somewhat larger than the entanglement distance d (marked by 1 in Fig. 1.1). The packing density of coiled macromolecules is lower than that of conformations with a parallel arrangement of molecular segments (in crystalline lamellae); the volume not filled by macromolecules (the unoccupied volume between the molecular segments) is termed the *free volume* and has a great influence on the mechanical properties of polymers in the amorphous state [3, 4].

It can be assumed that the meshes inside the entanglement network contain unentangled macromolecular segments, chain ends, or shorter macromolecules, which makes the interior of the meshes a little bit weaker than the entanglement network [5]. Such small density fluctuations are too small to make them visible by light scattering or in the electron microscope, but they can be revealed in deformed thin specimens of PS and SAN at the tip of crazes in the electron microscope in the so-called *precrazes*. Such a precraze is shown in Fig. 1.2(a), which consists of plastically deformed softer domains in front of a localized stress concentration. The precraze appears to be a broad band; however, the band is tilted in the specimen and is thinner than 100 nm, which has been demonstrated in Fig. I.68 in Part I by tilting the specimen in the microscope. An entanglement network with softer meshes and some of them stretched in a localized zone is sketched in Fig. 1.2(b). The comparison with the electron micrograph in Fig. 1.2(a) reveals the similarity of the domain structure of the precraze with the deformed meshes. The experimentally determined main distance between the domains of about 50 nm gives the average distance of larger, mechanically active meshes, convertible into precraze domains in the entanglement network. Using these results for strongly plastically stretched domains in PS, a *network model* of amorphous polymers was derived [6–8].

This network model was developed for PS with its relatively large entanglement distance d of about 10 nm and average mesh diameter D $(D = d\sqrt{2} \cong 1.4\,d)$ of about 14 nm. However, it can also be used for other amorphous polymers with smaller entanglement molecular weights and distances. These density fluctuations in a domain-like form are the weakest supramolecular structures in amorphous polymers. Therefore, the typical amorphous polymers, often used as models of an amorphous material, are also not really structureless. In the literature, there are some other results relating to the structures of amorphous polymers, ranging

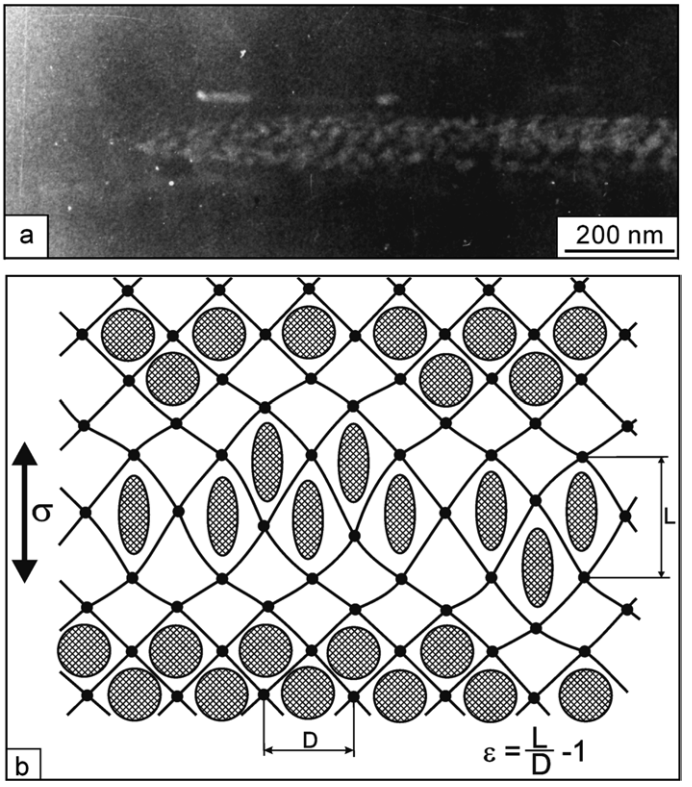

Figure 1.2 Comparison of

(a) a precraze structure in PS as visible in an HEM with

(b) a scheme of a network of entangled macromolecules with softer domain-like meshes, which are more strongly plastically stretched in an area of stress concentration

from very small microdomains (about 3 to 7 nm in diameter) to particles, globules, or density fluctuations in the range between 50 and 300 nm [9]. The problem is that such weak structural details produce only a very poor contrast, making them impossible to be investigated by scattering techniques and difficult to identify under the electron or atomic force microscope. Some of these details are visible only after a strong pretreatment of the material (e.g., surface etching, chemical attack, deformation at higher temperatures) [10] or using the effect of *strain-induced contrast enhancement* (see Chapter I.2, Fig. I.49) [9].

In the group of the single-phase amorphous polymers, PVC is an exception with a pronounced morphology with domains (about 100 nm) and so-called primary particles (about 1 μm) that are clearly visible in the electron microscope [11]. The interfaces between these structural details are preferential sites for chemical staining, highlighting the morphology of PVC (see Fig. 1.40).

Many thermoplastics, including glassy, brittle polymers, such as PS and PMMA, and ductile polymers, such as PVC and PC, are amorphous homopolymers; that is, they are composed of only one type of monomer. Copolymers and graft polymers, which are composed of two or more different types of monomers, do not show additional structures if they possess a statistical configuration (or alternating arrangement of the different monomers; see Fig. I.3). Deviations from the statistical arrangement of the monomers can yield microphase separations. An example is SAN when the composition of different macromolecules or macromolecular segments differs from the azeotropic one (76 mol.% S, styrene, 24 mol.% AN, acrylonitrile). Chain segments with lower S (styrene) content separate from their surroundings, forming about 100 nm small domains.

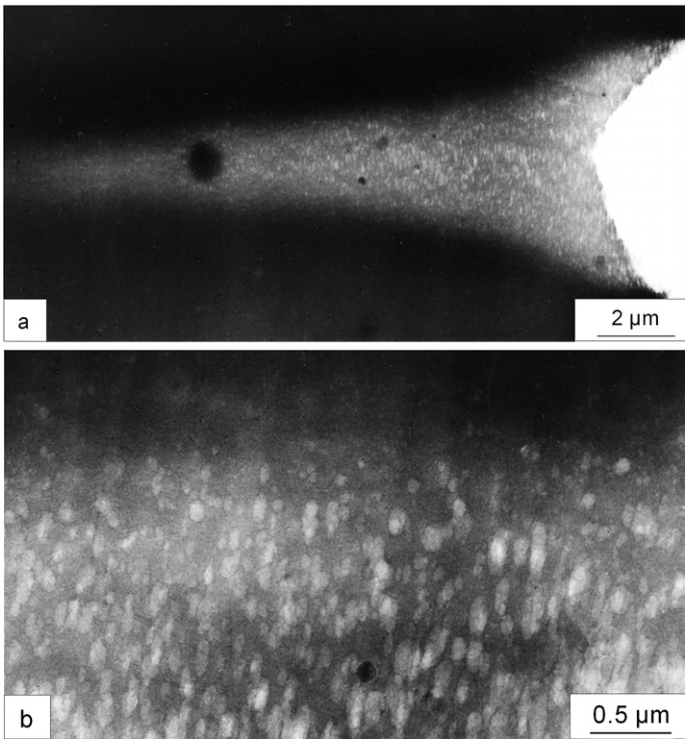

Figure 1.3 Craze-like deformation zone ahead of a crack tip in a SAN copolymer with strong plastically deformed (brighter) domains; these domains are somewhat softer than the surroundings because of a little bit changed composition of S:AN:

(a) overview;

(b) larger magnification;

(semithin section of SAN, deformed in an HEM, deformation direction vertical)

Polystyrene (PS)	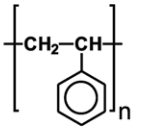
Polymethyl methacrylate (PMMA)	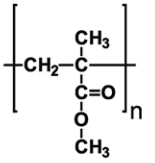
Polyvinyl chloride (PVC)	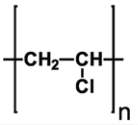
Polycarbonate (PC)	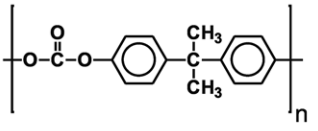
Styrene acrylonitrile (SAN)	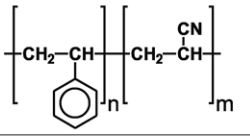
Cyclic Olefin Copolymer (COC) (Ethylene-norbornene Copolymer)	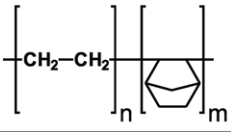

Table 1.1 Constitution of Some Typical Amorphous Polymers

1.2 Homopolymers

1.2.1 Polystyrene (PS)

Figure 1.13

PS tensile bar after loading with crazes;

top: overview; crazes are visible in reflected light as white lines perpendicular to the loading direction;

bottom: crazes in the tensile bar in low optical magnification, deformation direction horizontal; the tiny crazes are up to several 0.1 mm long;

light optical micrographs

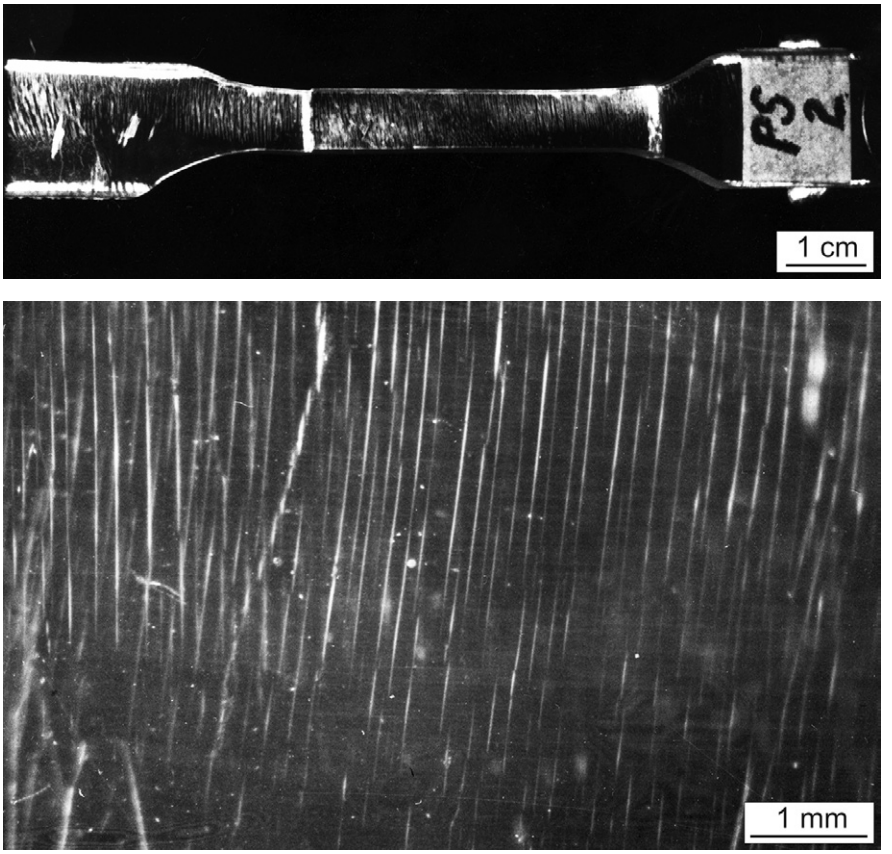

Figure 1.14

Overview of initiation zone of crazes at a surface notch in a deformed thin film in low magnification in TEM;

deformation direction horizontal

deformed semithin section, HEM

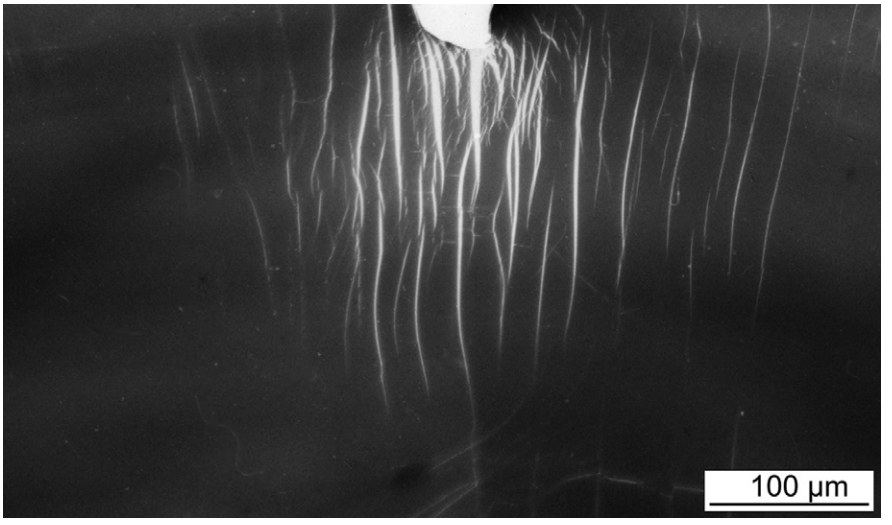

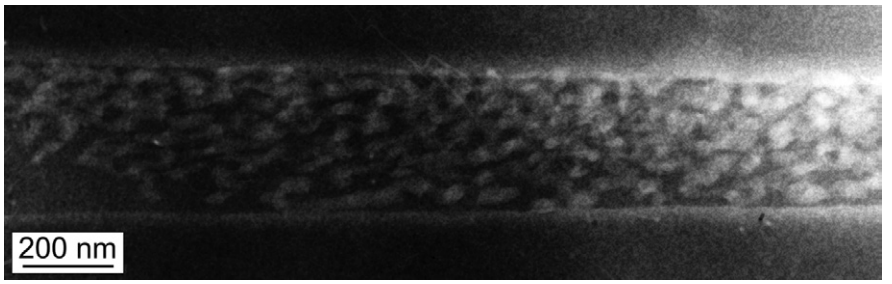

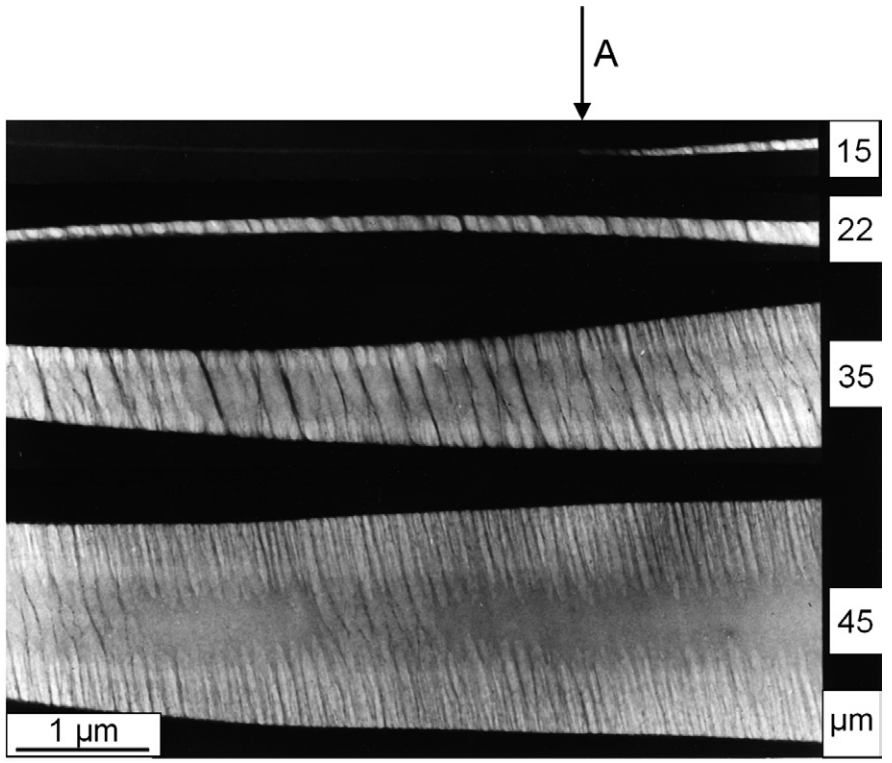

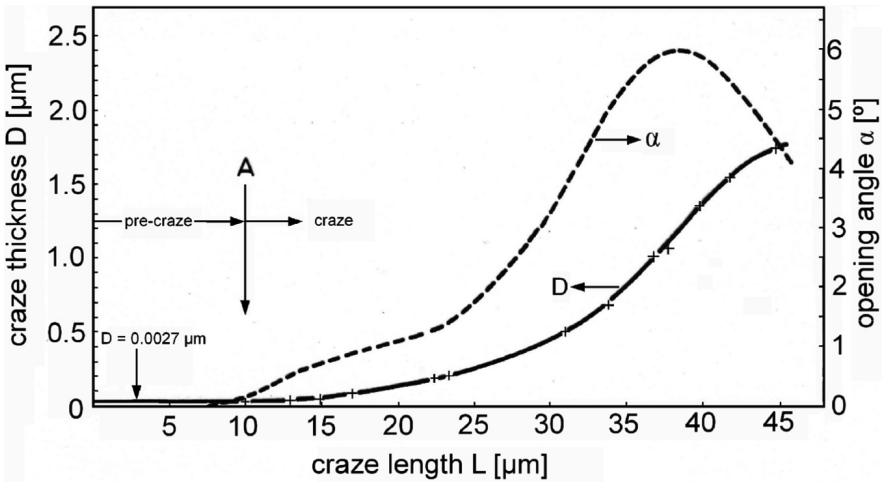

Figure 1.15

PS, change of craze details with growth in length and thickness [1–3];

top: precraze zone in front of the craze tip (left of mark "A" shown in micrograph below), consisting of small deformed domains; the precraze shown in the micrograph appears to be a broad band, but the band is tilted in the specimen and is thinner than 100 nm (see Fig. I.68 in Chapter I.3);

HEM micrograph

middle: structures of a craze at increasing distances from the craze tip; deformation direction vertical; "A" marks the transition of the precraze (about 30 nm thick) to the regular craze;

HEM micrographs

bottom: craze thickness profile: variation of craze thickness D and opening angle α with increasing craze length L; the precraze left of mark "A" is about 30 nm thick and 10 μm long; crazes are up to some μm thick with an opening angle α becoming smaller with increasing craze length;

Figure 1.16

PS film, deformed;

precraze domains in front of a craze tip, deformation direction perpendicular; the smallest deformed domains in the precraze are about 20–50 nm in diameter (similar to the deformed and ruptured meshes of the entanglement network; see Fig. 1.2);

thin film, deformed, HEM

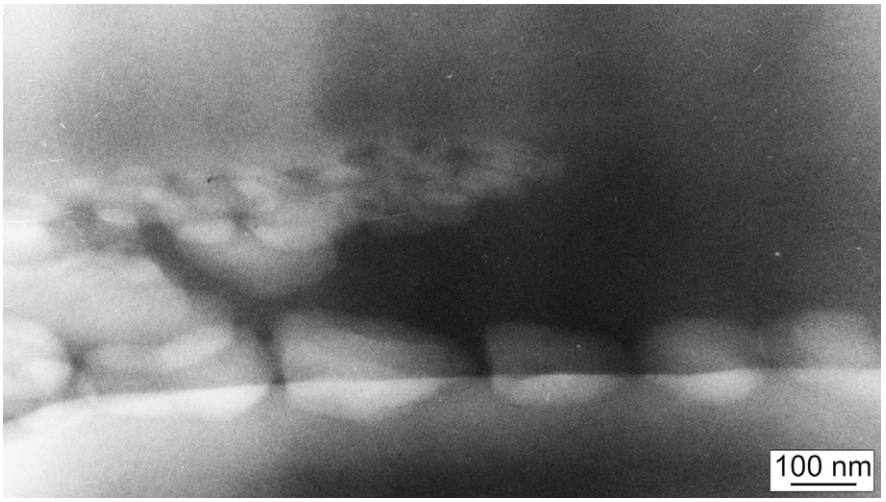

Figure 1.17

PS, interior of a longer craze with clear fibrillation [1, 3];

fibrils are oriented in the direction perpendicular to the craze boundaries and parallel to the loading direction, and they consist of strongly plastically deformed material up to elongations between 100 and 400%; between the fibrils, elongated nanovoids appear with a void content of up to more than 50%; therefore, crazing is associated with an increase in volume and a decrease in material density;

deformed thin PS film in HEM

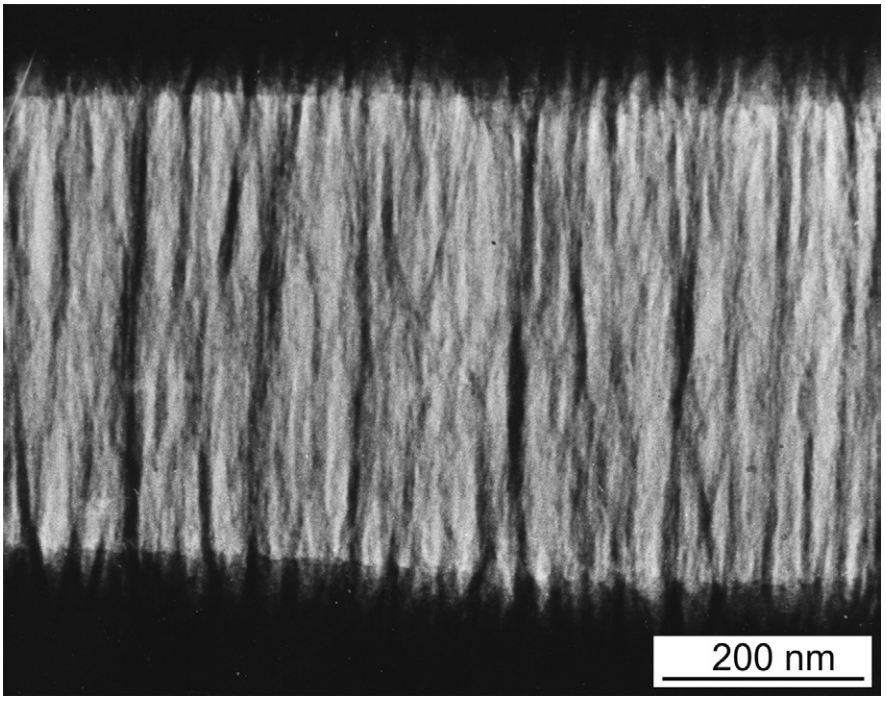

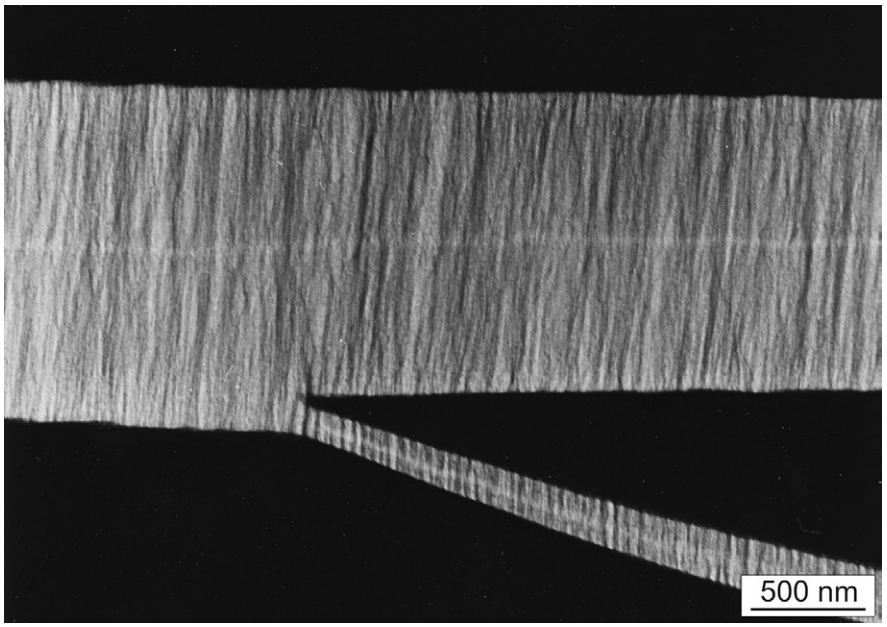

Figure 1.18

PS, interior of a craze;

regular fibrillation with a side craze; thickness of the fibrils between 2 and 10 nm with a long period of about 15 nm; in the middle of the craze a narrow brighter zone exists, the "mid-rib," which contains a somewhat higher void content and results from originally locally larger stresses at the craze tip (the higher stresses at the craze tip initiate the transformation of the macromolecular entanglement network into the fibrillar craze structure (see Figs. 1.2 and 1.6);

deformed PS film (1 μm thick) in HEM

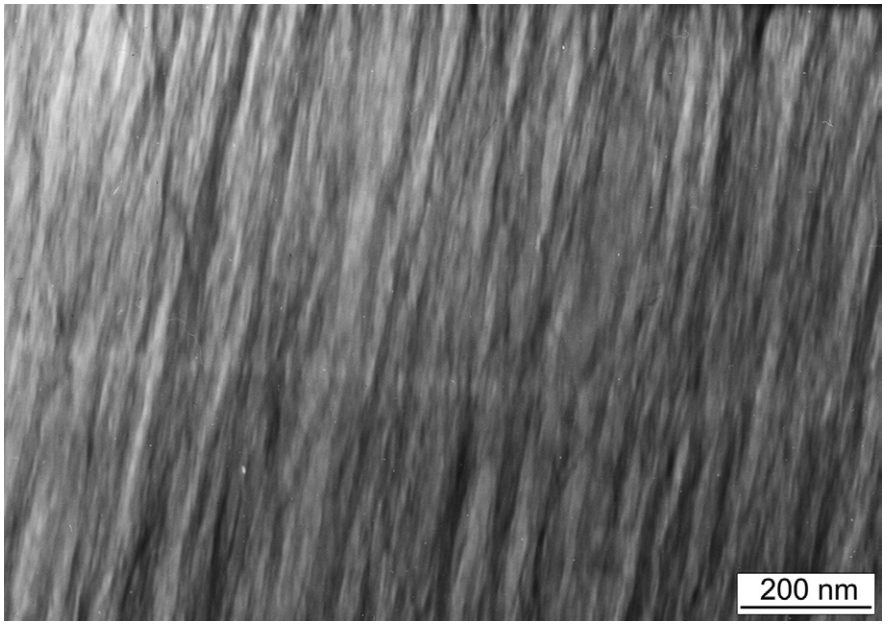

Figure 1.19

PS, larger magnification of the interior of a craze;

the apparently visible "fibrils" are shorter dark strips and superposition structures of many true fibrils (in the direction of the electron beam there are many fibrils that cannot be resolved individually); the smallest visible distances of stripes correlate with the average distances between craze fibrils [1];

deformation direction vertical, HEM

Figure 1.20

PS, larger magnification of a fibrillated craze;

relatively sharp transition from the interior of the fibrillated craze to the undeformed polymer material (at the top); the fibrils are formed at the craze-bulk interphase due to the *pull-out mechanism* (see scheme in Fig. 1.7);

deformed thin section, HEM

Figure 1.21

PS, craze in deformed bulk material;

deformation direction vertical, after deformation chemically stained with osmium tetroxide; the nanovoids inside the craze are filled with the chemical staining agent, appearing black;

ultrathin section, TEM

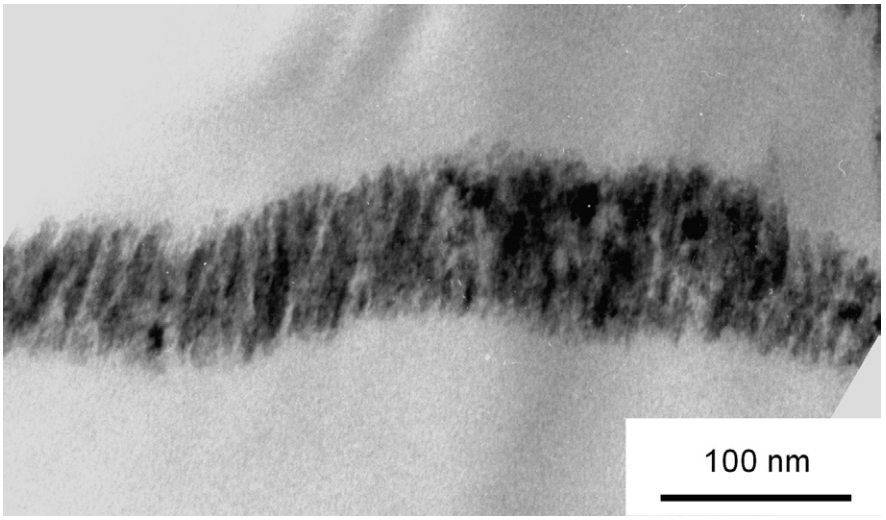

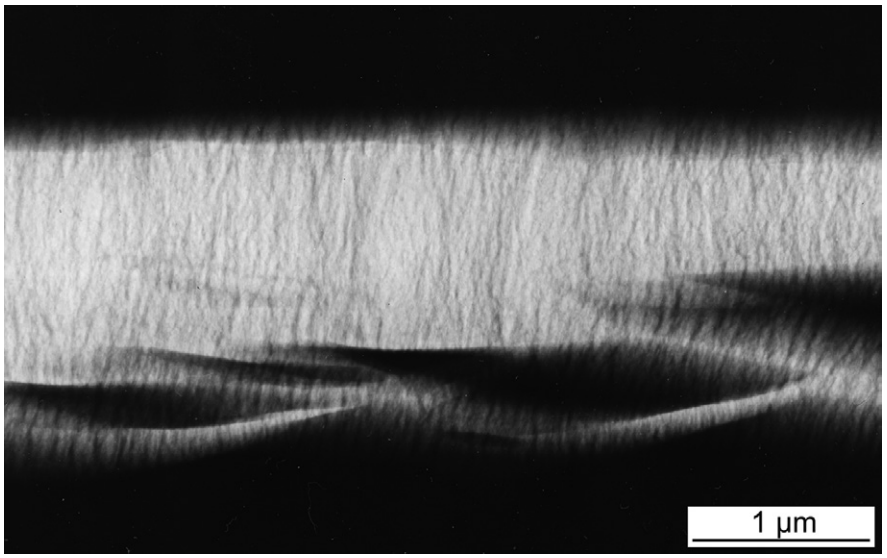

Figure 1.22(a)–(c)

PS, deformed, different structures of crazes;

(a) craze with fine fibrils and smaller fibrillated side crazes, deformation direction vertical;

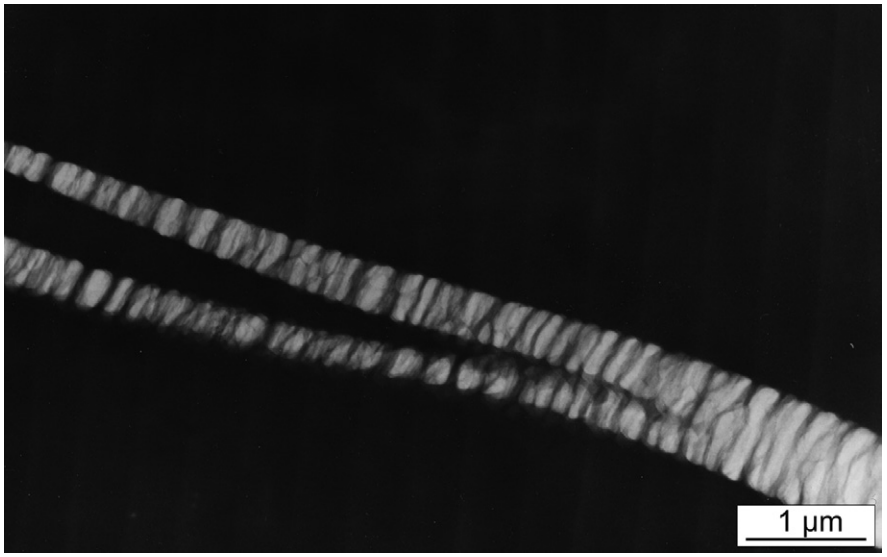

(b) craze with larger voids and thicker fibrils (coarse craze);

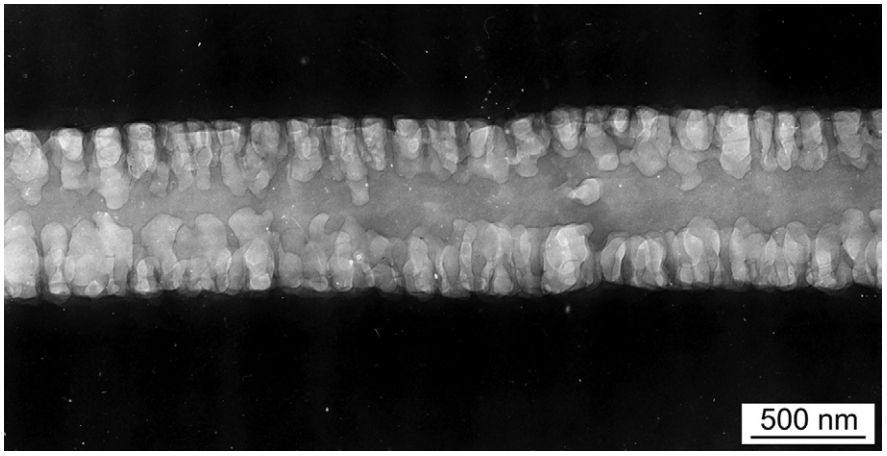

(c) craze with larger voids at the craze boundaries and homogeneously deformed material inside, deformation direction vertical;

1–2 µm thick sections from bulk PS, 1 MeV HEM

CHAPTER 4

Polymer Blends

4.1 Overview

Polymer blends consist of a combination of two or more different polymers. They are called "blends," "polymer mixtures," or "polymer combinations" because they are mainly created using a process of mixing or blending. Mixing of two or more polymers can be performed either in the molten or the solution state or by in situ polymerization of a monomer in the presence of a dissolved polymer. The original reasons for preparing polymer blends were to create a polymer that has a desired combination of the different properties of its components. This idea is illustrated by curve (a) in Fig. 4.1, which represents the simple combination of a property of polymer A with the corresponding property of polymer B for various compositions (this curve is termed the *additivity line*). One precondition of this case is that the polymer components are compatible or that incompatibility between the components is not too large. Curve (b) illustrates the usual case of simple mixing of different incompatible polymers. The deterioration of the property is due to large demixing morphologies and a low phase adhesion. Therefore, improving compatibility between the different polymers and optimizing the morphology are the main issues to address when producing polymer blends. Curve (c) shows an improvement in this property within a special composition range (it rises above the level of the additivity line (a)), but there is a decrease in the property below the additivity line within another composition range. Curve (d) illustrates a synergistic effect, which produces a property that is better than the properties of either of the polymer components.

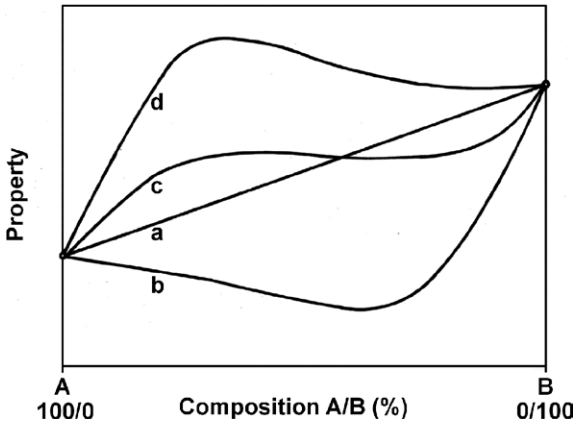

Figure 4.1 Variation of a blend property with composition for blends of two polymers A and B, different cases:

(a) "additivity line," compatible mixed components;

(b) incompatible components, worsening of properties;

(c) partial improvement of properties;

(d) synergistic effects

This effect requires polymer blends with well-defined morphologies and optimum micromechanisms. The preparation and study of the morphology and properties of polymer blends have been one of the major areas of polymer research in the past decades. A number of books and detailed reviews have been published on this subject [1–5]; an excellent overview on the micro- and nanostructure of polymer blends is [5].

4.1.1 Morphology

The morphology of polymer blends is determined by the incompatibility of the polymer components, which causes phase separation, and the processing (e.g., shear forces during mixing, viscosities, temperature). In the following, an overview of some typical morphologies is presented. Incompatible polymers, such as PS with PE or PP, usually show strong phase separation with the formation of large particles; see Fig. 4.2(a) and (b). Often, the minor component forms particles (here PS), which are dispersed within the major component, forming the matrix (PP). Under load, cracks follow the particle interface, debonding particles from the matrix and unveiling the spherical shape of the PS particles. When 3% PP/PS block copolymer is added, it covers the particles and improves contact with the matrix; see Fig. 4.2(c) and (d). The weakest part is no longer the interface, so cracks also propagate across PS particles.

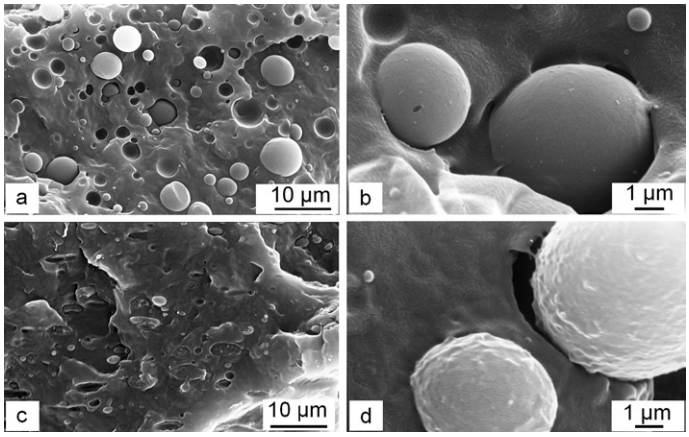

Figure 4.2 Phase separation in PP/PS blends (composition 85%/15%):
(a), (b) without compatibilizer;
(c), (d) with 3% PP/PS block copolymer used as compatibilizer;
(fracture surfaces, SEM micrographs)

Several mechanisms are used to enhance the compatibility and interfacial strength between the polymer phases, including mixing with compatibilizers (block copolymers, graft polymer), reactive blending, or grafting. Compatibilization causes a reduction in the particle size of the minor component in the matrix. Figure 4.3 shows blends of PA 66 and syndiotactic PS without (micrograph (a)) and with (micrograph (b)) 10% sPS/PA modifier [6]. The large sPS particles in the blend without modifier (micrograph (a)) are drastically reduced in size and better linked to the matrix when 10% modifier is added (see Fig. 4.52 in Section 4.3).

Grafting of PS onto LDPE via γ irradiation allows the formation of small PS domains in the LDPE matrix; see Fig. 4.4. The smallest PS domains of about 40 nm in micrograph (a) correspond to PS macromolecular coils with molecular weights of about 10^6; coiled PS macromolecules between PE lamellae are sketched in Fig. 4.4(b). As the degree of grafting increases, the PS domains grow in size; see Fig. 4.31 [7].

The morphology of a blend is more complex when each of the polymer components possesses its own morphology or when more than two components exist. Figure 4.5 shows smaller details of the phase morphology of a PA/ABS blend (volume ratio 70/30) in a chemically stained ultrathin section in TEM. The rubber particles inside the SAN domains of the ABS component are strongly chemically fixed and stained with OsO_4 and thus appear black. The PA matrix is stained with formalin/OsO_4,

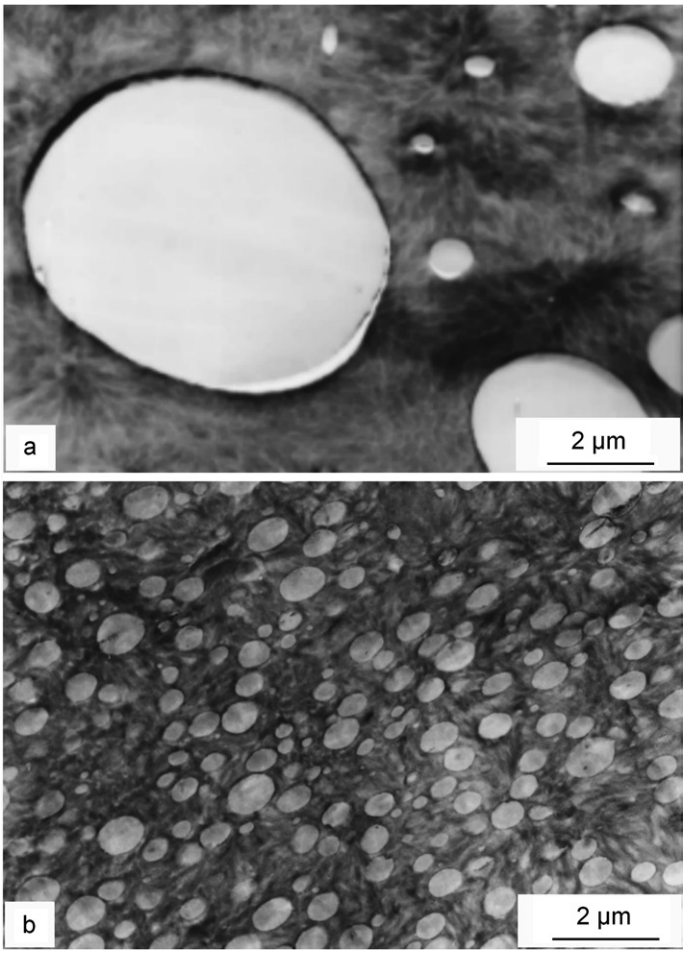

Figure 4.3 Influence of a compatibilizer on the morphology of PA 66/sPS blends:

(a) PA 66/sPS (80/20) blend without compatibilizer;

(b) PA 66/sPS (70/20) with 10% compatibilizer;

(selectively stained ultrathin sections, TEM) [6]

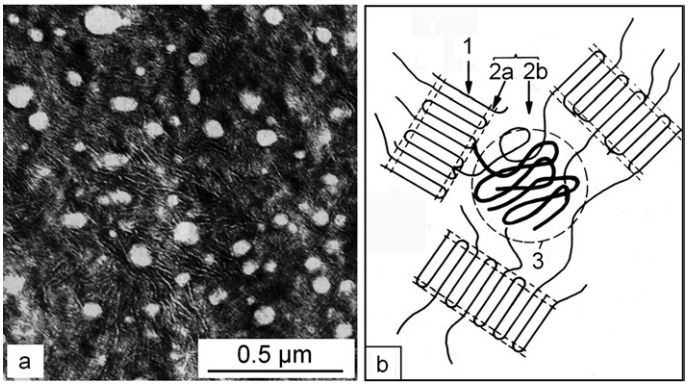

Figure 4.4 PS/LDPE blends after grafting styrene onto PE with small PS particles (bright) in the LDPE matrix; grafting efficiency 10% [7]:

(a) selectively stained ultrathin section, TEM;

(b) sketch of coiled PS macromolecules (3) in the interlamellar regions (2b) between crystalline lamellae (1) with lamellae interphases (2a)

appearing gray. Besides the larger ABS particles, many small SAN particles with diameters below a few hundreds of nanometers are visible [8].

A distribution of small PS particles embedded in a PE network can be realized up to much more than 50% PS following the route of polymerization of styrene in PE. Figure 4.6 shows such a network arrangement with small PS domains of a blend with a high content of 90% PS and only 10% PE. In the dark PE parts, small lamellae are visible (see also Figs. 4.32 and 4.33 in Section 4.3) [9].

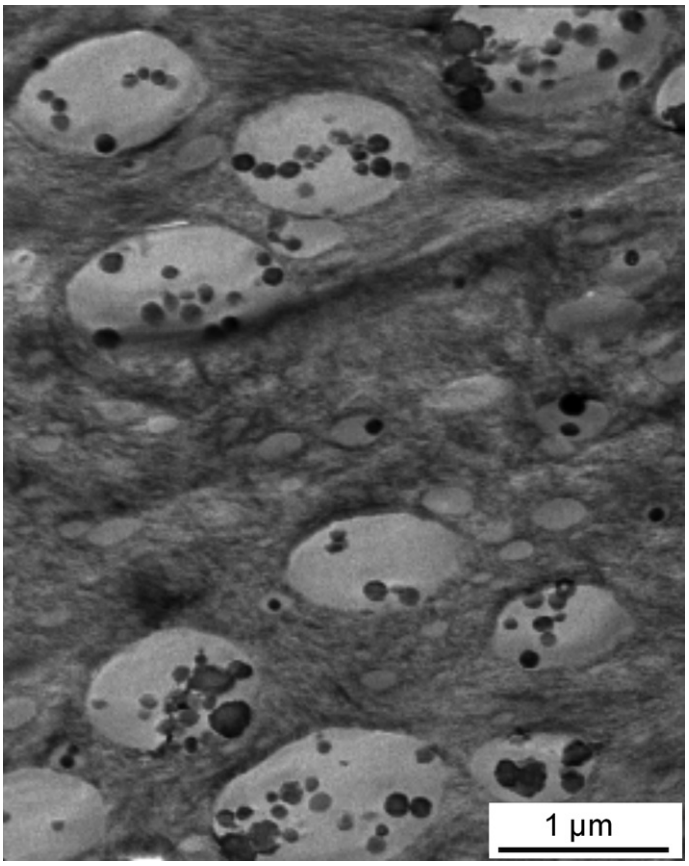

Figure 4.5 Visibility of several different phases in a PA/ABS (70/30) blend: chemical fixation and staining reveal larger ABS particles (SAN with PB rubber) in the PA matrix (with small SAN domains and PA lamellae) [8] (staining of rubber with OsO_4 and of PA with formalin/OsO_4, ultrathin section, TEM)

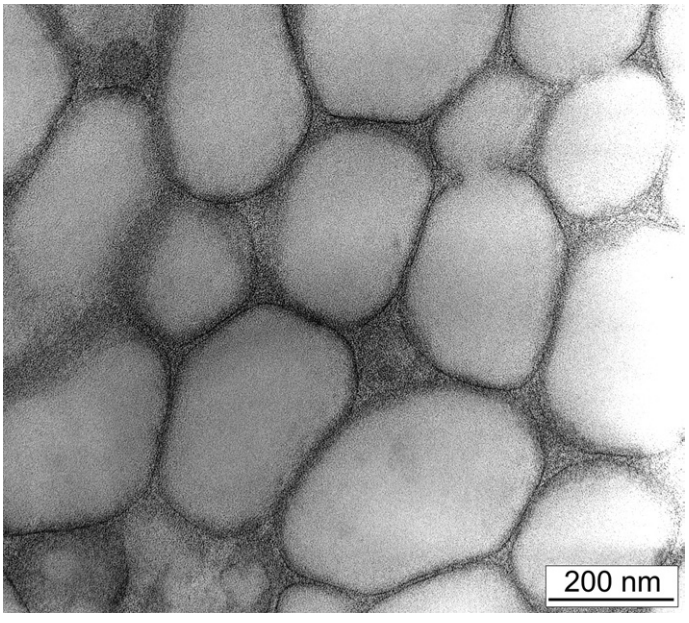

Figure 4.6 Network morphology of a PS/PE (90/10) blend with smaller PS particles in a PE network (stained, ultrathin section, TEM) [9]

A weaker phase separation appears in blends of similar semicrystalline polymers. Figure 4.7 shows the phase morphology of an LDPE/HDPE/PP (75/20/5) blend in two magnifications with a separate PP phase in the form of bright particles.

4.2 Blends of Amorphous Polymer Components

There are only a few compatible polymer blends without a pronounced morphology, such as PS/PPO or SAN/PMMA. The morphology of the other blends of amorphous polymers is determined by their incompatibility and processing conditions. Occasionally it can be difficult to reveal the morphology of an amorphous polymer blend in detail if there are no clear interface boundaries or the components show no different staining abilities—in such cases some special preparation techniques are used.

The following polymer blends are presented: PC/MBS, PC/ABS, PC/PMMA, PMMA/PB, PC/SAN, and epoxy/SBS

4.2.1 Morphology of the Blends

Figure 4.15(a)(b)

PC/MBS blend (98/2), composition 98% PC, 2% MBS:

(a) lower magnification: butadiene rubber particles from MBS appear black and are dispersed in the PC matrix;

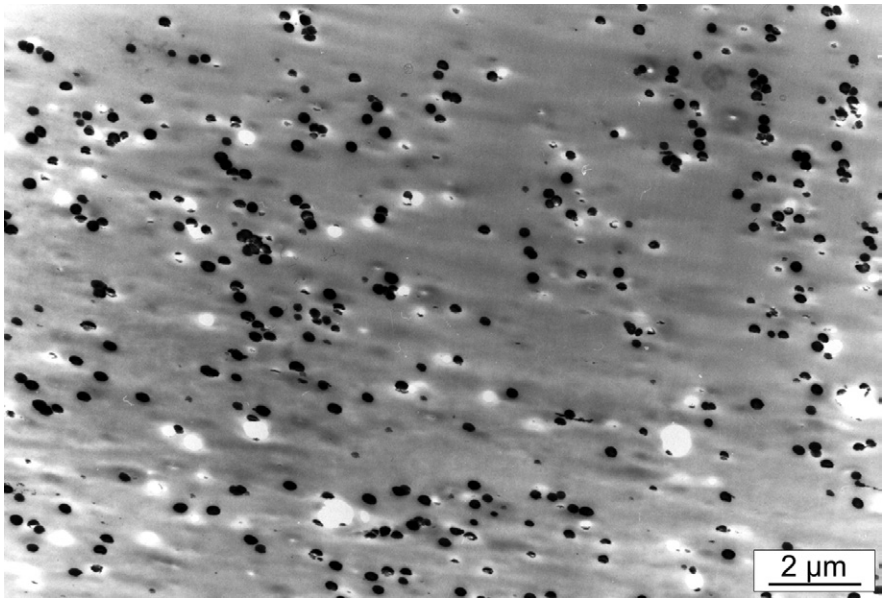

(b) larger magnification: spherical PB rubber particles (black) from MBS distributed in the PC matrix; no contrast between poly(methyl methacrylate) styrene and PC is visible;

chemically stained with OsO_4 at 60 °C, UDS, TEM,

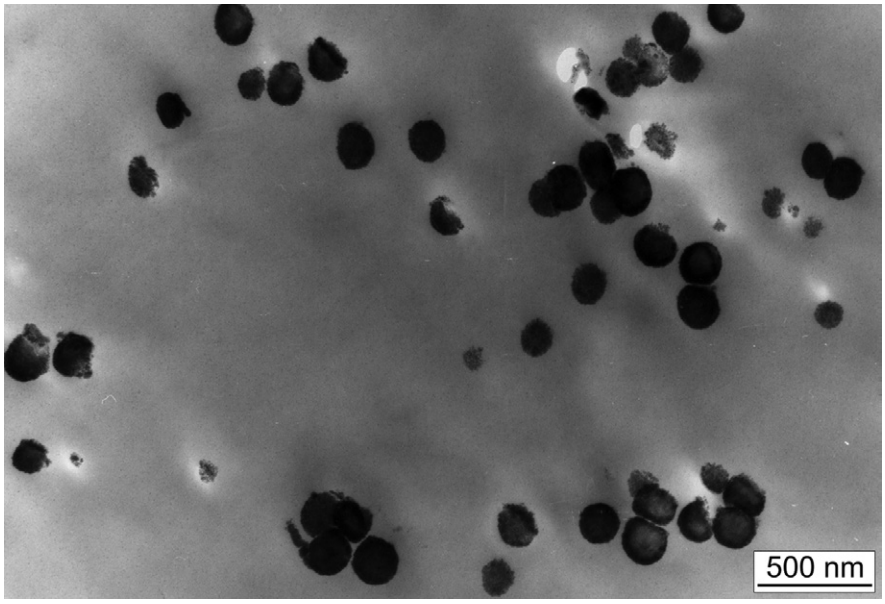

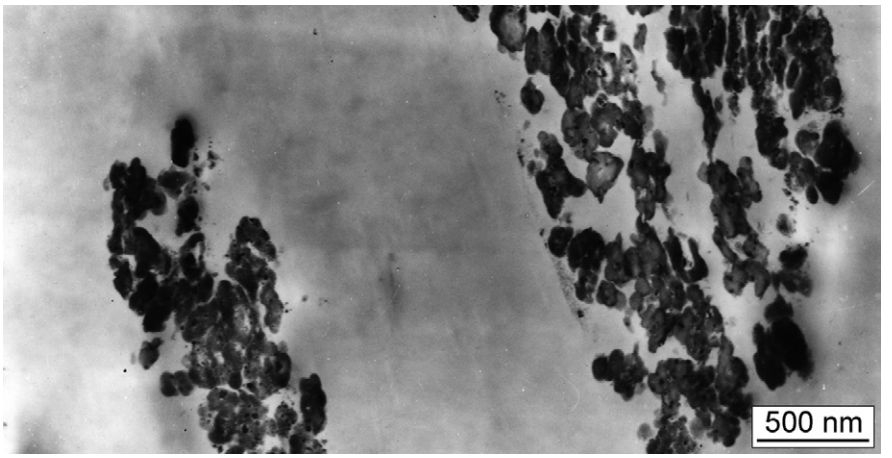

Figure 4.16

PC/ABS (90/10) blend;

ABS domains distributed in the PC matrix; in the ABS domains, rubber particles appear black and are distributed in SAN surroundings; only a very weak contrast appears between PC matrix and SAN;

chemically stained with OsO_4, UDS, TEM

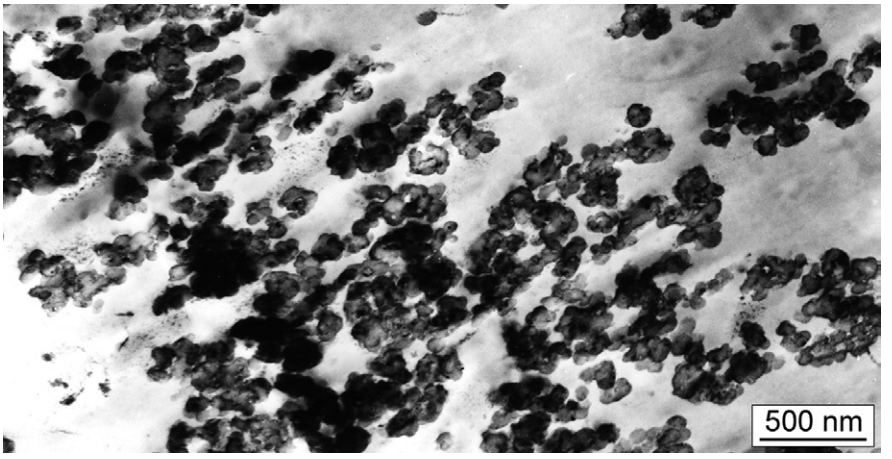

Figure 4.17

PC/ABS (30/70) blend;

in the ABS matrix (rubber particles dark), irregularly shaped PC particles (bright) are distributed without an interface layer;

chemically stained with OsO_4, UDS, TEM

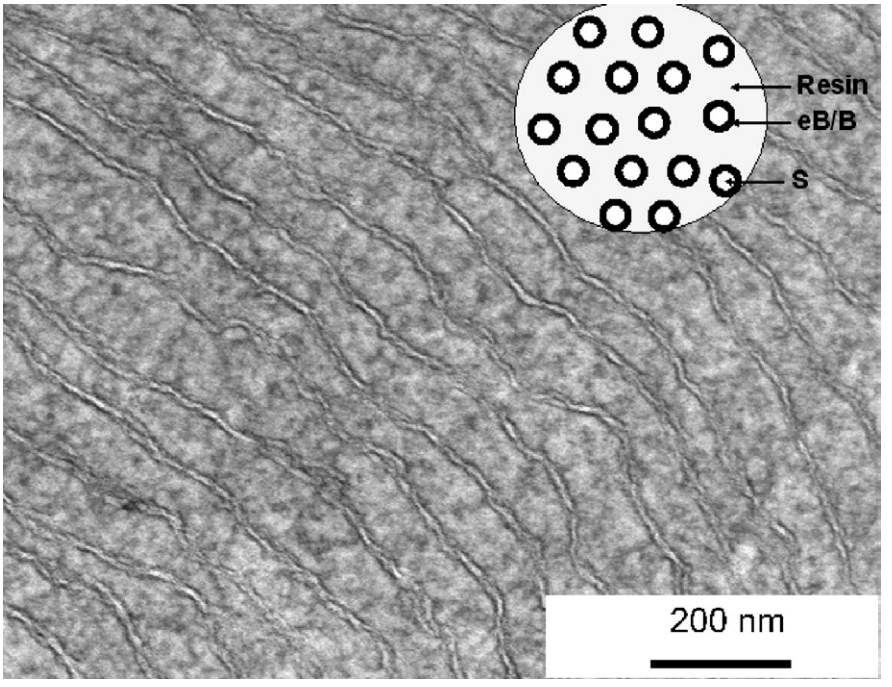

Figure 4.18

Epoxy resin with 30 wt.% epoxidized SBS (styrene butadiene) star-block copolymer [1];

epoxidation of SBS using meta-chloroperoxybenzoic acid improves compatibility; the insert sketches the morphology with PS cylinders (S) embedded in the shell of epoxidized butadiene (eB/B) surrounded by epoxy resin;

chemically stained with OsO_4, UDS, TEM

Figures 4.19–4.20 PC/PMMA (60/40) blend, different preparation techniques

Figure 4.19

Cocontinuous morphology;

PC phase is dark, PMMA bright, each continuous phase incorporates dispersed particles of the other phase [2];

usual OsO_4 staining, UDS, TEM

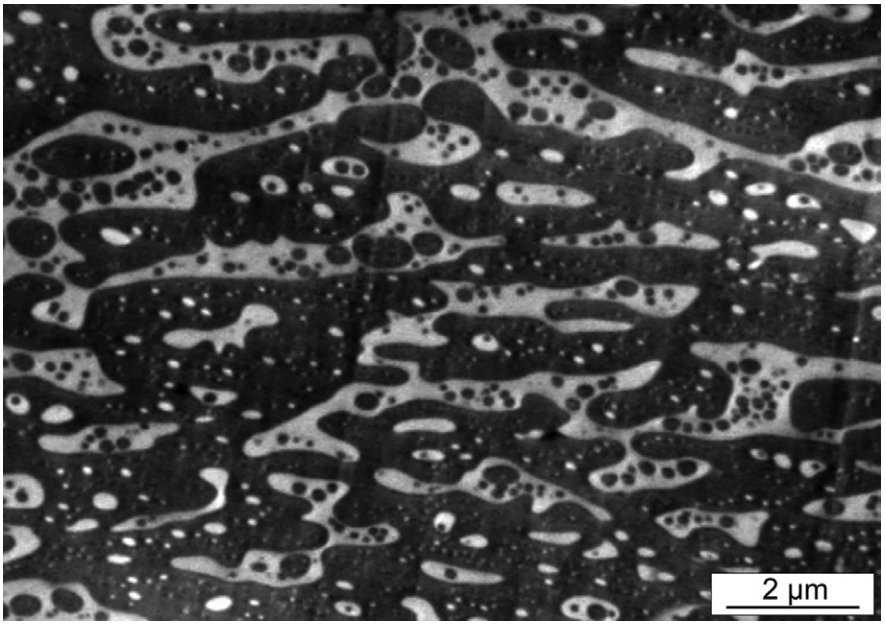

Figure 4.20

Visibility of the cocontinuous morphology by volume relaxation without etching;

ultramicrotomed surface at low temperature, annealed at 150°C; smooth background is PC, irregular textures are PMMA (effect of PMMA, not of PC) [3a];

cut surface, annealing, SEM

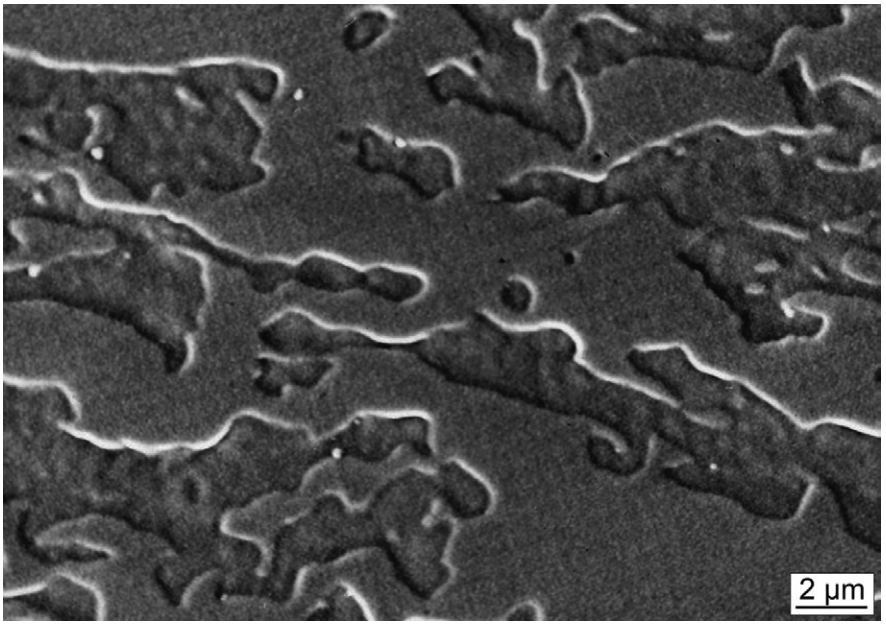

Figures 4.21–4.23 PC/SAN blends, different preparation techniques

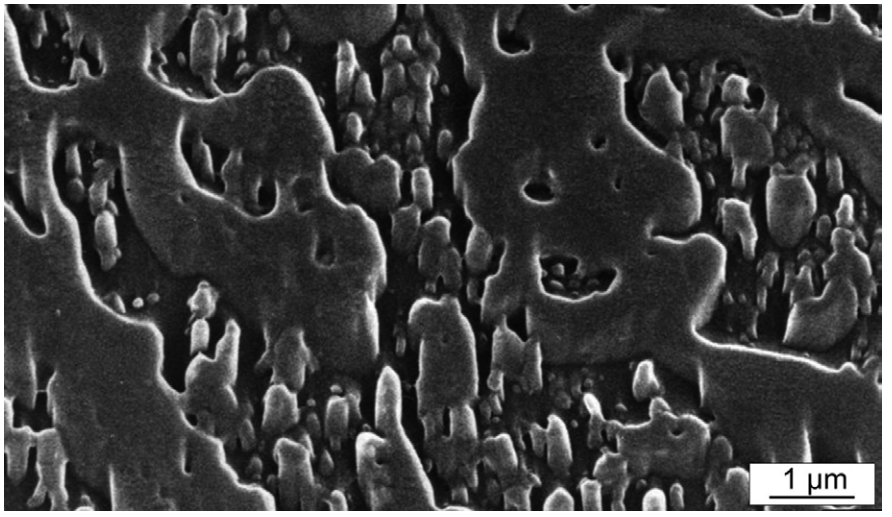

Figure 4.21

PC/SAN (50/50):

visibility of the cocontinuous morphology by etching an ultramicrotomed surface with a modified permanganic mixture (1% $KMnO_4$ in H_2SO_4), etching time 50 min; SAN is etched off, and remaining even areas are PC [2];

cut surface, sputter coating with Pt, SEM

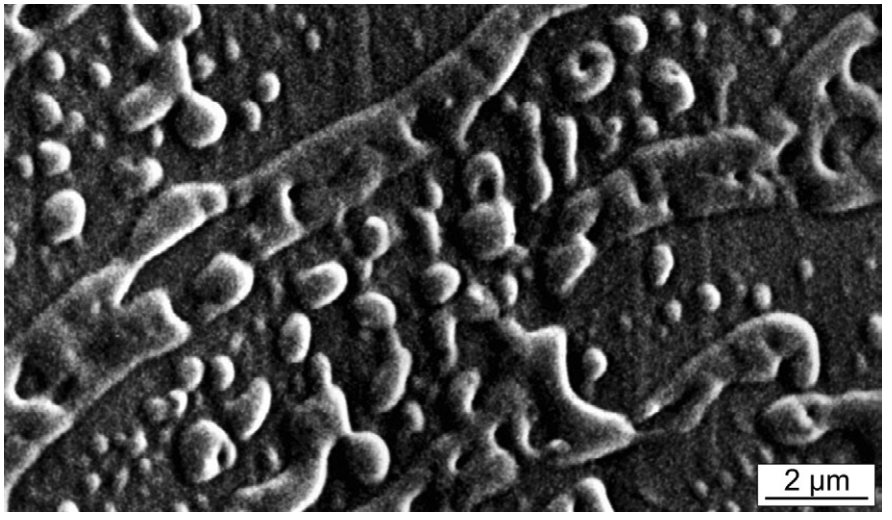

Figure 4.22

PC/SAN (60/40) phase structure revealed by selective swelling of one of the constituents (SAN);

ultramicrotomed cut surface is subjected to vapors of a liquid concentrated acetic acid that can selectively interact with the minor component [3b];

Au layer, SEM

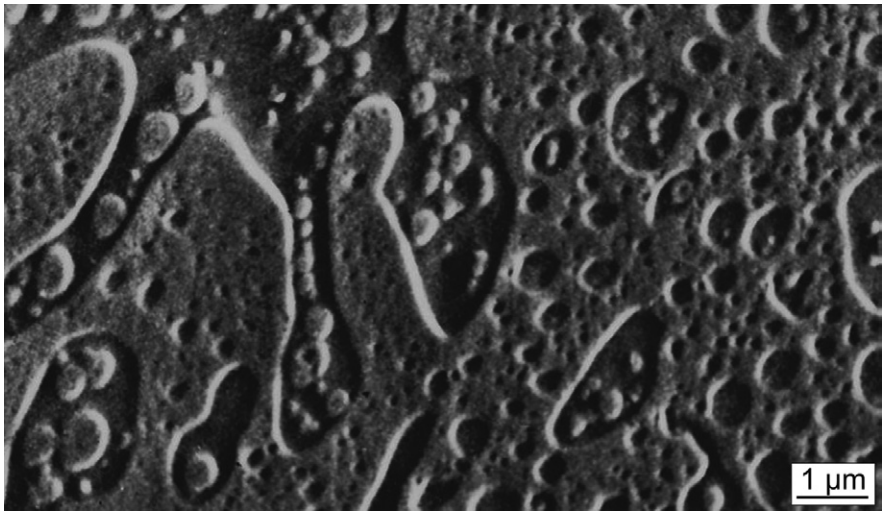

Figure 4.23

PC/SAN (60/40) phase structure revealed by volume relaxation method;

ultramicrotomed cut surface; annealing of the sample at 140°C results in shrinking of the SAN phase while the PC remains unchanged [3b];

10 nm Au layer, SEM

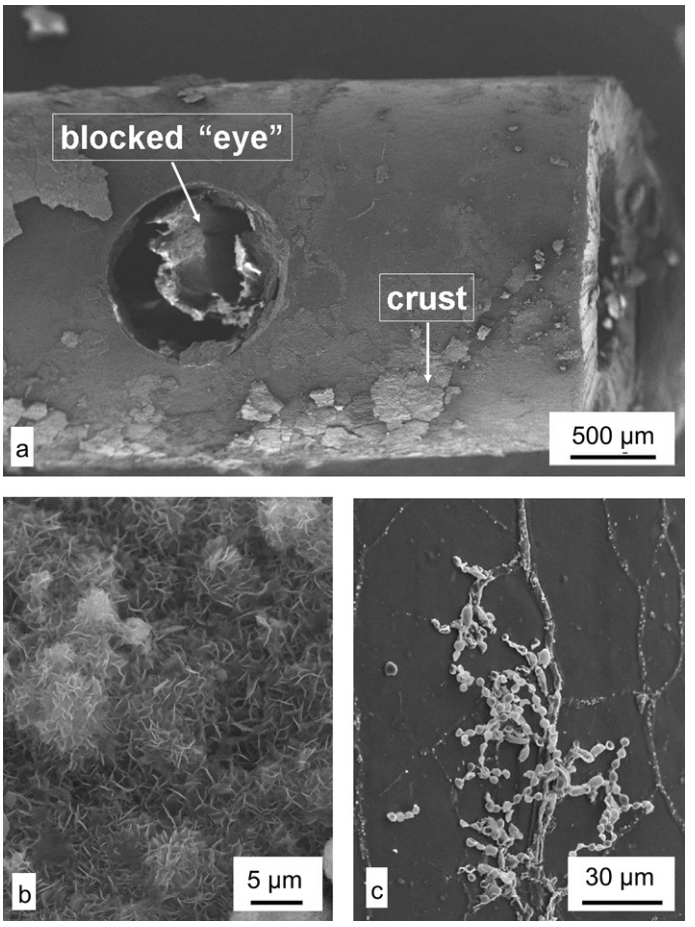

Figure 8.5 Ureter stent with incrustations:

(a) overview of the end of the stent with a hole (“eye”) and parts of a compact crust;

(b) detail of the crust surface;

(c) surface of the stent with microorganisms; surface coated with carbon, SEM micrographs [14]

In hip and knee joints, UHMWPE is used for polymer inlays in metal-back hip cups bearing the artificial femoral head of metal alloys or ceramics and separate the upper and lower metallic parts of the artificial knee. With metallic and ceramic counterparts, UHMWPE exhibits a very low friction coefficient, exceptional wear resistance, and long-term dimensional and chemical stability [17]. Although UHMWPE is considered to be bioinert and does not induce immunogenic or inflammatory reactions of the host tissue, continuous wear may cause severe damage sometimes leading to implant failure and revision surgery. Therefore, UHMWPE implants have only a limited lifetime in the range of 15 years [17]. Abrasion of UHMWPE particles can induce foreign body reactions in the surrounding tissue, leading to aseptic loosening of the prostheses. Additional surface damaging or even cracks of polymer components require immediate surgery. Despite the recognized success and worldwide acceptance of total joint arthroplasty, wear is a major obstacle limiting the longevity of implanted UHMWPE components.

Knee-joint prostheses consist of two metal components that replace the destroyed joint surfaces of the thigh bone (femur) and the shinbone (tibia) and that are usually cast from cobalt- or titanium-based alloys. The tibia part is typically extended by a short stem, anchoring the system in the marrow cavity. A UHMWPE insert is used as the articulating counterpart to optimize sliding behavior and to minimize wear; see Fig. 8.6.

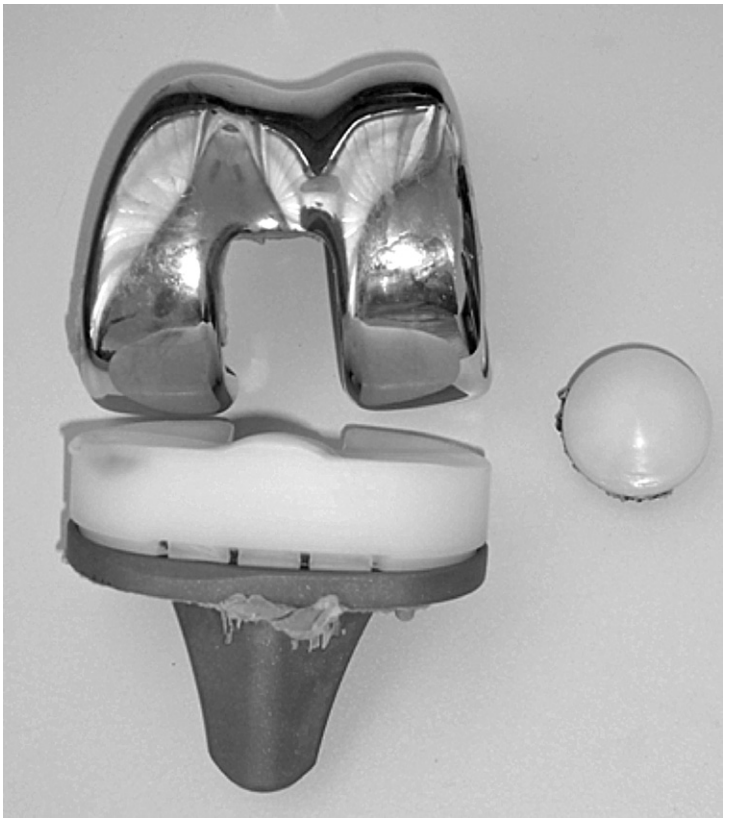

Figure 8.6 Knee arthroplasty with upper and lower metallic parts and a plastic spacer of UHMWPE

The fixation of the implant parts in the bone may be achieved by self-curing polymer resins (bone cements) such as PMMA (see above) or via direct integration of micro- or macroporous implant surfaces into the host bone. The UHMWPE used for knee and hip joints is usually highly cross-linked [17].

There are several producers of knee implants, who manufacture them by different fabrication technologies and with different properties of the UHMWPE component in the prostheses, which can influence the service life of an implant. Not only from an economic but also from the medical point of view, a marked increase in longevity is necessary, and this requires an improvement of the artificial replacements and its material, including UHMWPE. One possibility is improvement of the compaction of the UHMWPE powder to a better compacted solid without visible interfaces between the individual powder particles (see Figs. 2.49–2.52 in Section 2.2.2 and Figs. 8.43 and 8.45 in Section 8.3).

Different defect types in knee implants have been investigated using light optical and scanning electron microscopy inspection. Based on the microscopic investigation, a classification of characteristic defect types of the inlays of knee implants has been performed to understand better the mechanical damaging mechanisms [18]. One example is illustrated in Fig. 8.7 with the surface of a damaged UHMWPE inlay from a total knee prosthesis after revision surgery with defects in the form of scratches (region 1 in Fig. 8.7(a) and (b)) and of an eroded region with pits (region 2 in Fig. 8.7(a) and (c)) [14]. From such regions, UHMWPE parts can be abraded and induce reactions in the surrounding tissue, leading to aseptic loosening of the prostheses. Some more examples are shown in Figs. 8.42–8.46.

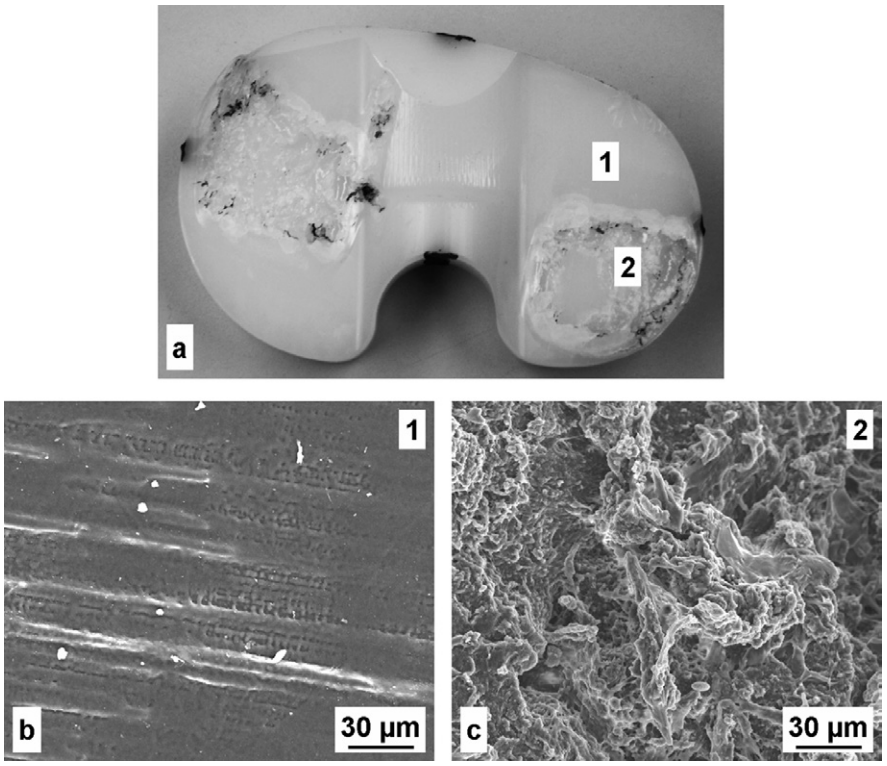

Figure 8.7 Surface of a UHMWPE inlay with defects from a total knee prosthesis:

(a) optical micrograph of an explanted inlay with two marked regions 1 and 2,

(b) detail from region 1 showing scratches,

(c) detail from region 2 with an eroded area and pits;

SEM images [13, 17]

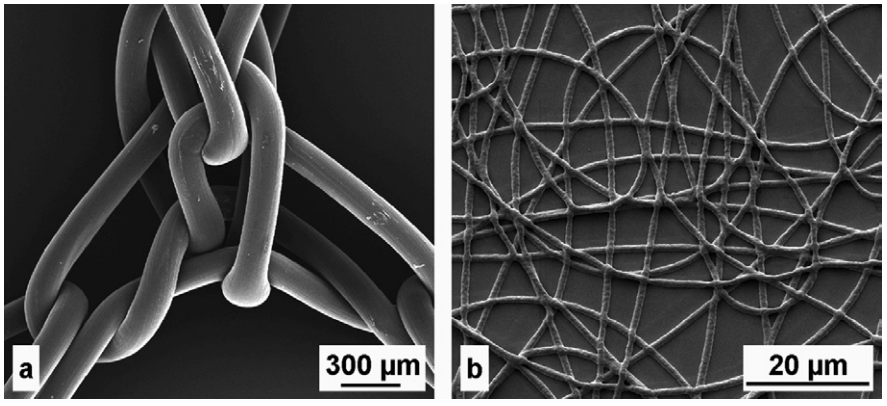

Figure 8.8 Comparison of different mesh-like structures:

(a) PP fibers used for mesh prostheses,

(b) nonwoven PHB scaffold produced by electrospinning;

SEM images [14]

Polymers are also used as surgical suture material, meshes, and scaffolds. Figure 8.8 provides a comparison of two kinds of mesh-like structures. Mesh prostheses from polypropylene fibers like those shown in Fig. 8.8(a) are used to support overstressed and weakened tissue (such as in the treatment of abdominal hernias). In this case the material must be bioinert. Completely different systems consist of much finer micro- or nanofibers produced by electrospinning; see Fig. 8.8(b). They are used as substrates for tissue engineering and consist of bioresorbable polymers like PHB and PLLA (polylactid acid). Because of their small diameters, they have a relatively large surface area. The bioactivity can be improved by functionalization or by adding drugs or other bioactive components. SEM imaging of the surfaces of sutures or scaffolds provides information on fiber diameter, mesh size, degradation, and biofilm formation. Figure 8.9 shows a typical woven suture

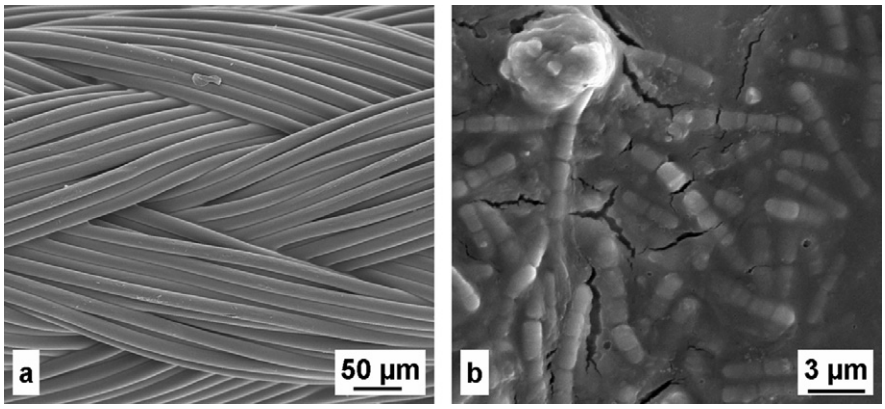

Figure 8.9 Woven surgical suture in the original state (micrograph (a)) and after a few days of service in the oral cavity (micrograph (b)); SEM images [14]

before use in micrograph (a) and after application for several days in the oral cavity with a biofilm on it in micrograph (b).

Electrospun nanofibers possess unique properties that cannot be found in conventional fibers. They have extraordinarily high surface area per unit mass, high permeability, low basis weight, high cost effectiveness, and superior directional strength, among other properties (see Section 9.4). These properties also make the nonwoven nanofibers appropriate materials for widespread applications in medicine. In particular, the nanofibers are found to mimic the structure, chemical composition, and mechanical properties of the native extracellular matrix (ECM) [19, 20]. Therefore, nanofiber-based scaffolds are considered to be interesting materials in the field of skin tissue engineering, bone regeneration, wound healing, vascular grafts, and drug delivery systems [21].

The skin is the largest organ of the human body, providing many different functions, including protection against heat, injury, and infections [21]. Therefore, failure or complete loss of the skin is incompatible with sustained life. The ideal tissue-engineered skin should as closely as possible approximate the skin in nature and function. Nanofibers from PVA/PHB (hydrophilic/hydrophobic) blend polymers with different ratios as scaffolds have been fabricated for skin tissue engineering [22]. Another clinical need is identification of new bone materials to replace or restore the function of traumatized, damaged, or lost bone. Recently, studies on three-dimensional scaffold materials have become a key element of bone tissue engineering. Collagen and hydroxyapatite have the potential to mimic natural ECM and replace diseased or destroyed skeletal bones. The combination of both ceramic and polymer within one composite material will provide the ductility of the polymer and the bioactivity of the calcium phosphate phase. Nanocomposite nanofiber scaffolds consisting of PVA/Col with hydroxyapatite nanoparticles unidirectionally aligned using an electrospinning technique have been fabricated to mimic the nanostructure of human bone tissue [23–25]; see Figs. 8.50–8.55.

There are other applications of polymers in medicine, such as membranes for blood purification or separation of blood components, medical disposal (syringes, catheters, blood bags, sanitary products), dental fillings, resorbable bone nails, drug delivery systems, hydrogels, and different products for clinical diagnostics.

References for 8.1

1. Jennissen, H.P., *Bionanomaterials* (report from the German DGM Fachausschuß) (2010) 11(S1) p. 110
2. Aichmayer, B., Fratzl, P., *Physik J.* (2010) 9, pp. 33–38
3. Shi, B., Shlepr, M., Palfery, D., *J. Appl. Polym. Sci.* (2011) 120, pp. 1808–1816
4. Imam Khasim, H.R., Henning, S., Michler, G.H., Brandt, J., *Macromol. Symp.* (2010) 294, pp. 144–152
5. Reddy, N., Yang, Y., *Innovative Biofibers from Renewable Resources* (2015) Springer-Verlag, Berlin
6. Bhandari, N.L., Mormann, W., Michler, G.H., Adhikari, R., *Mater. Res. Innovations* (2013) 17, pp. 250–256
7. Michler, G.H., Baltá-Calleja, F.J., *Nanomechanics and Micromechanics of Polymers: Structure Modification and Improvements of Properties* (2012) Carl Hanser Verlag, Munich, Section 12.4, "Biopolymers," pp. 539–555
8. Das, M., Chakraborty, D., *J. Appl. Polym. Sci.* (2009) 112, pp. 447–453; 489–495
9. Hristov, V.N., Krumova, M., Vasileva, S., Michler, G.H., *J. Appl. Polym. Sci.* (2004) 92, pp. 1286–1292
10. Niaounakis, M., *Biopolymers* (2014) Elsevier, New York
11. Wintermantel, E., Ha, S.-W., *Biokompatible Werkstoffe und Bauweisen - Implantate für Medizin und Umwelt*, 5th ed. (2009) Springer-Verlag, Berlin
12. Kühn, K.D., *Bone Cements. Up-to-date Comparison of Physical and Chemical Properties of Commercial Materials* (2000) Springer-Verlag, Berlin
13. Henning, S., Ph.D. Thesis (2006) Martin Luther University Halle-Wittenberg
14. Michler, G.H. (Ed.), *Electron Microscopy of Polymers* (2008) Springer-Verlag, Berlin, Heidelberg, Chapter 23, "Biomaterials," pp. 429–443
15. Dette, K.-E., Michler, G.H., Hey, I., Asran, A.S., Arnold, C., German Patent (2010) DE 10 2010 007 956.1 (Patent title: Verfahren zur Herstellung eines dauerhaften Verbundes zwischen Ethylenvinylacetat (EVA) als Weichplastmaterial und Polymethylmethacrylat (PMMA) für herausnehmbaren Zahnersatz)
16. Henning, S., Haberland, E.J., Kluge, A., Burkert, S., Michler, G.H., Bloching, M., *Biomaterialien* (2005) 6(S1), p. 74
17. Kurtz, S.M., *The UHMWPE Handbook: Ultra-high Molecular Weight Polyethylene in Total Joint Replacement* (2004) Elsevier Academic Press, San Diego, California
18. Michler, G.H., Baltá-Calleja, F.J., *Nano- and Micromechanics of Polymers: Structure Modification and Improvement of Properties* (2012) Carl Hanser Verlag, Munich, Section 12.3, "Biomedical Polymers," pp. 512–539
19. Asran, A.S., Michler, G.H., Kim, G.-M., Seydewitz,V., *Textile Processing: State of the Art & Future Developments*, 6th Intern. Conf. of Textile Research Division NRC, Cairo, Egypt, April 5–7 (2009) 6, pp. 18–25
20. Asran, A.S., Salama, M., Popescu, C., Michler, G.H., *Macromol. Symp.* (2010) 294, pp. 53–161

21. Leung, V., Ko, F., *Polym. Adv. Technol.* (2011) 22, pp. 350–365

22. Asran, A.S., Razghandi, K., Aggarwal, N., Michler, G.H., Groth, T., *Biomacromolecules* (2010) 11, pp. 3413–3421

23. Asran, A.S. Henning, S., Michler, G.H., *Polymer* (2010) 51, pp. 868–876

24. Henning, S., Khasim, H.R.I., Michler, G.H., Brandt, J., *Macromol. Symp.* (2012) 315, pp. 84–97

25. Asran, A.S., Sänger, T., Laub, M., Michler, G.H., Henning, S., Jennissen, H.P., *Biomed. Tech.* (2014) 59, DOI 10.1515/bmt-2014-4030

8.2 Biobased Polymers

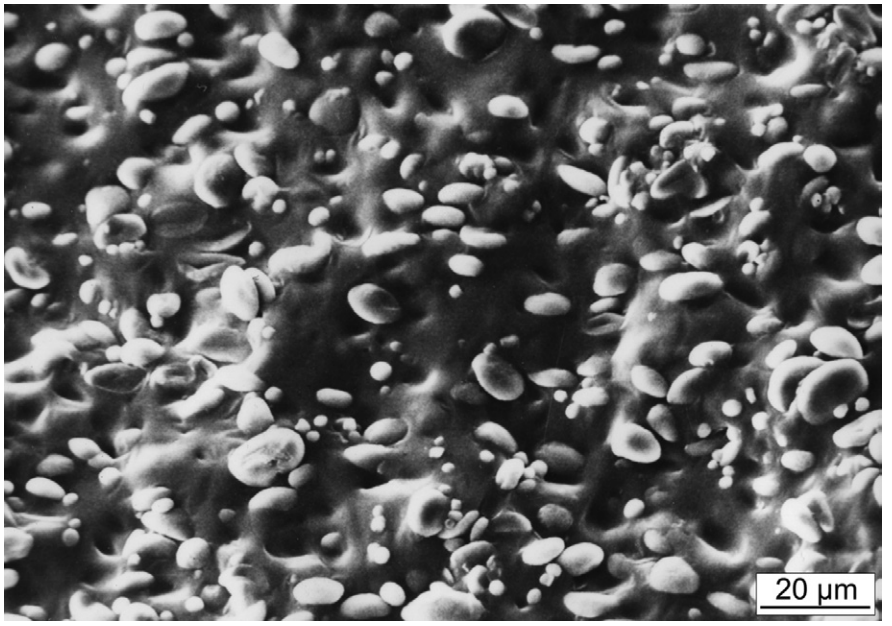

Figure 8.10

Starch/EVA (50%/50%) blend;

blend of starch and EVA with 80% vinyl acetate (VA) content: irregularly shaped starch particles in the EVA matrix;

brittle fracture surface, coated, SEM

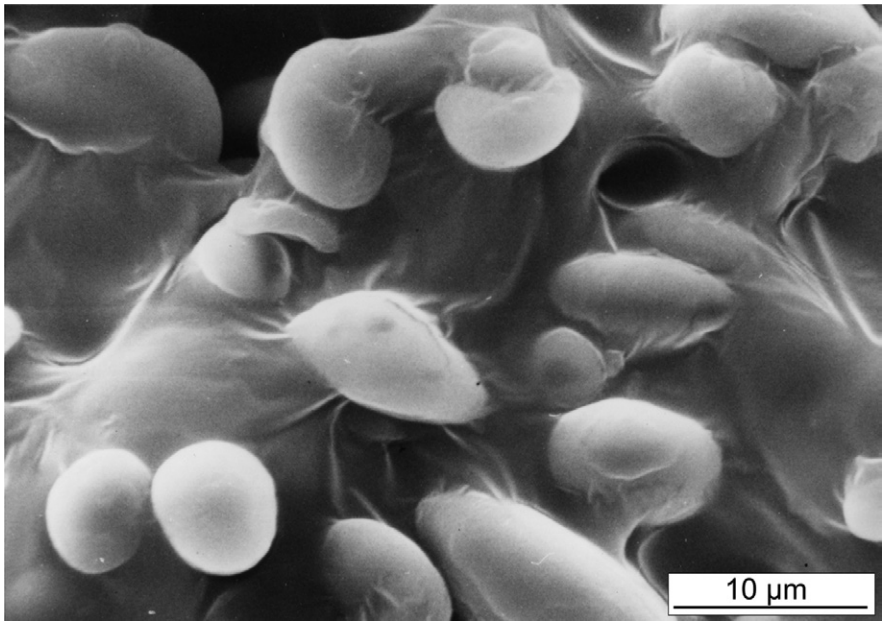

Figure 8.11

Starch/EVA/glycerol (45%/45%/10%) blend;

blend with well-bonded starch particles in the EVA matrix;

brittle fracture surface, coated, SEM

Figure 8.12

Starch/EVA (70%/30%) blend;

higher content of starch than in material of Fig. 8.10, larger starch particles with higher concentration in the EVA matrix;

brittle fracture surface, coated, SEM

Figure 8.13

Starch/EVA (50/50) blend, deformed;

starch particles debonded from the EVA matrix, cavitation and void formation around particles, ductile deformation of EVA matrix strands;

fracture surface, coated, SEM

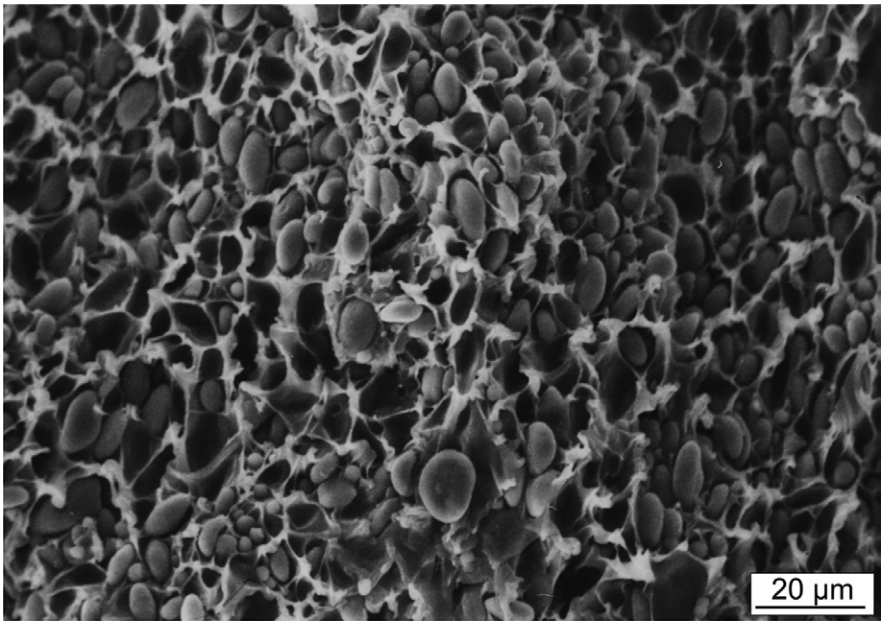

Subject Index